Goddard Cumulus Ensemble (GCE) model: Application for understanding precipitation processes

Wei-Kuo Tao

Laboratory for Atmospheres
NASA/Goddard Space Flight Center
Greenbelt, MD 20771

AMS Meteorological Monographs

Symposium on Cloud Systems, Hurricanes and TRMM

(August 24, 2000)

Corresponding author address: Dr. Wei-Kuo Tao, Mesoscale Atmospheric Processes Branch, Code 912, NASA/GSFC, Greenbelt, MD 20771
email: tao@agnes.gsfc.nasa.gov

1. Introduction

The global hydrological cycle is central to climate system interactions and the key to understanding their behavior. Rainfall and its associated precipitation processes are a key link in the hydrologic cycle. Fresh water provided by tropical rainfall and its variability can exert a large impact upon the structure of the upper ocean layer. In addition, approximately two-thirds of the global rain falls in the Tropics, while the associated latent heat release accounts for about three-fourths of the total heat energy for the Earth's atmosphere (Riehl and Simpson 1979). Precipitation from convective cloud systems comprises a large portion of tropical heating and rainfall. Furthermore, the vertical distribution of convective latent-heat releases modulates large-scale tropical circulations (e.g., the 30-60-day intraseasonal oscillation - see Sui and Lau 1988), which, in turn, impacts midlatitude weather through teleconnection patterns such as those associated with El Niño. Shifts in these global circulations can result in prolonged periods of droughts and floods, thereby exerting a tremendous impact upon the biosphere and human habitation. And yet, monthly rainfall over the tropical oceans is still not known within a factor of two over large (5-degrees latitude by 5-degrees longitude) areas (Simpson *et al.* 1988, 1996). Hence, the Tropical Rainfall Measuring Mission (TRMM), a joint U.S./Japan space project, can provide a more accurate measurement of rainfall as well as estimate the four-dimensional structure of diabatic heating over the global tropics. The distributions of rainfall and inferred heating can be used to advance our understanding of the global energy and water cycle. In addition, this information can be used for global circulation and climate models for testing and improving their parameterizations.

Cloud resolving (or cumulus ensemble) models (CRMs) are one of the most important tools used to establish quantitative relationships between diabatic heating and rainfall. This is because latent heating is dominated by phase changes between water vapor and small, cloud-sized particles, which can not be directly detected using remote sensing techniques (though some passive microwave frequencies do respond to path-integrated cloud water). The CRMs, however, explicitly simulate the conversion of cloud condensate into raindrops and various forms of precipitation ice. It is these different forms of precipitation that are most readily detected from space, and which ultimately reach the surface in the form of rain in the Tropics. In addition, the highest science priority identified in the Global Change Research Program (GCRP) is the role of clouds in climate and hydrological systems, which have been identified as being the most problematic issues facing global change studies. For this reason, the GEWEX (Global Energy and Water Cycle Experiment) formed the GCSS (GEWEX Cloud

System Study), specifically for the purpose of studying such problems. CRMs were chosen as the primary approach (GCSS Science Plan 1993; Moncrieff et al. 1997).

The first pioneering one dimensional cloud model was developed by Dr. J. Simpson in the 1960s. A two-dimensional anelastic model that filtered out sound waves was developed by Drs. Y. Ogura and N. Phillips. The models were used to study cloud development under the influence of the surrounding environment. The 1D cloud model was used extensively to study the cloud seeding problem. In the late 1970's, four three-dimensional cloud models were developed (Wilhelmson 1974; Miller and Pearce 1974; Sommeria 1976; Clark 1979; Klemp and Wilhelmson 1978; Cotton and Tripoli, 1978; and Schlesinger 1975, 1978). The effect of model designs (i.e., slab vs axis-symmetric, and 2D vs 3D) on cloud development and liquid water content were the major foci in 70's. Also, the dynamics of midlatitude supercells, that are usually associated with tornados, was another major focus in the 70's. After GATE, cloud ensemble modeling was developed to study the collective feedback of clouds on the large-scale tropical environment with the aim of improving cumulus parameterization in large-scale models (i.e., Tao 1978; Soong and Tao 1980; Tao and Soong 1986; Lipps and Helmer 1986; Krueger 1988). The effect of ice processes on cloud formation and development, stratiform rain processes and their relation to convective cells, and the effect of wind shear on squall line development were the other major areas of interest for cloud resolving models in the 1980's. The impact of radiative processes on cloud development was also investigated in the late 80's. In the 1990's, cloud resolving models were used to study multi-scale interactions, cloud chemistry interaction, idealized climate variations, and surface processes. The cloud resolving model was also used for the development and improvement of satellite rainfall retrieval algorithms. Table 1 lists the major foci and some (not all) of the key contributors to cloud resolving model development over the past four decades.

During the past 20 years, observational data on atmospheric convection has been accumulated from measurements by various means, including radars, instrumented aircrafts, satellites, and rawinsondes in special field observations (e.g., GATE, PRE-STORM, COHMEX, TAMEX, EMEX, TOGA COARE[1] and several others). This has made it possible

1 GATE stands for GARP (Global Atmospheric Research Program) Atlantic Tropical Experiment, TAMEX for Taiwan Area Mesoscale Experiment, EMEX for Equatorial Mesoscale Experiment, PRE-STORM for Preliminary Regional Experiment for Storm Central, COHMEX for Cooperative Huntsville Meteorological Experiment, and TOGA COARE for Tropical Oceans Global Atmosphere (TOGA) - Coupled Ocean Atmosphere Response Experiment (COARE).

for cloud resolving modelers to test their simulations against observations, and thereby improve their models. In turn, the models have provided a necessary framework for relating the fragmentary observations and helping to understand the complex physical processes interacting in atmospheric convective systems, for which observations alone still cannot provide a dynamically consistent four-dimensional picture. The past decades have also seen substantial advances in the numerical modeling of convective clouds and mesoscale convective systems (e.g., squall-type and non-squall-type convective systems), which have substantially elucidated complex dynamical cloud-environment interactions in the presence of varying vertical wind shear. With the advent of powerful scientific computers, many important and complex processes (which require extensive computations), such as ice-microphysics and radiative transfer, can now be simulated to a useful (but still oversimplified) degree in these numerical cloud models. Table 2 lists the key developments in the cloud resolving model approach for studying *tropical* convection over the past two decades. As shown, over the last 20 years, these models have become increasingly sophisticated through the introduction of sophisticated (bulk-type) microphysical processes, radiation and boundary-layer effects, and improved turbulent parameterizations for subgrid-scale processes. In addition, an exponentially increasing computer resource has resulted in time integrations increasing from hours to days, domain grids boxes (points) increasing from less than 2000 to more than 2,500,000, and 3-D models becoming increasingly prevalent. The CRM is now at a stage where it can provide reasonably accurate statistical information of the sub-grid, cloud-resolving processes now poorly parameterized in climate models and
numerical prediction models.

2. Goddard Cumulus Ensemble (GCE) Model

The Goddard Cumulus Ensemble (GCE) model is a cloud resolving model, and its main features have been published by Tao and Simpson (1993) and Simpson and Tao (1993). The model is nonhydrostatic and model variables include horizontal and vertical velocities, potential temperature, perturbation pressure, turbulent kinetic energy, and mixing ratios of all water phases (vapor, liquid, and ice). The cloud microphysics includes a parameterized Kessler-type two-category liquid water scheme (cloud water and rain), and a three-category ice-phase scheme (cloud ice, snow and hail/graupel) mainly based on Lin *et al.* (1983) and Rutledge and Hobbs (1984). The Goddard microphysics scheme has several minor modifications, however. The first modification is the option to choose either graupel or hail as the third class of ice (McCumber *et al.* 1991). Graupel has a low density and a large intercept (i.e., high number concentration). In contrast, hail has a high density and a small intercept (i.e. low number concentration). These differences can affect not only the description of the hydrometeor population, but also the relative importance of the microphysical-dynamical-radiative processes. Second, a saturation technique was implemented by Tao *et al.* (1989b). This saturation technique is basically designed to ensure that supersaturation (subsaturation) cannot exist at a grid point that is clear (cloudy). This saturation technique is one of the last microphysical processes to be computed. It is only done prior to evaluating the evaporation of rain and snow/graupel/hail deposition of sublimation. A third difference is that all microphysical processes (transfer rates from one type of hydrometeor to another) are calculated based on one thermodynamic state . This ensures that all processes are treated equally. The opposite approach is to have one particular process calculated first modifying the temperature and water vapor content (i.e., through latent heat release) before the second process is computed. The fourth difference is that the sum of all the sink processes associated with one species will not exceed its mass. This ensures that the water budget will be balanced in the microphysical calculations.

The following major improvements have been made to the model during the past seven year period: **(i)** The implementation of a multi-dimensional Positive Definite Advection Transport Algorithm (MPDATA, Smolarkiewicz and Grabowski 1990). All scalar variables (potential temperature, water vapor, turbulence coefficient and all hydrometeor classes) use forward time differencing and the MPDATA for advection. The dynamic variables, u, v and w, use a second-order accurate advection scheme and a leapfrog time integration (kinetic energy semi-conserving method). **(ii)** The development of an improved four-class, multiple-moment, multiple-phase ice scheme (Ferrier 1994), which resulted in improved agreement with observed radar and hydrometeor structures for convective systems simulated in different geographic locations without the need for adjusting coefficients (Ferrier *et al.* 1995). **(iii)** The inclusion of solar and infrared radiative transfer processes, which have been used to study the impact of radiation upon the development of clouds and precipitation (Tao *et al.* 1991, 1996) and upon the diurnal variation of rainfall (Tao *et al.* 1996; Sui *et al.* 1998) for tropical and midlatitude squall systems. **(iv)** The incorporation of land and ocean surface processes to investigate their impact upon the intensity and development of organized convective systems (Wang *et al.* 1996; Lynn *et al.* 1998). Mesoscale circulations, which formed in response to landscape heterogeneities represented by a land surface model, were crucial in the initiation and organization of the convection.

A stretched vertical coordinate (height increments from 40 to 1150 m) is used to maximize resolution in the lowest levels of the model. Typically, a total of 1024 grid points are used in the horizontal with 500-1000m resolution in the two-dimensional version of the GCE model. In the three-dimensional version of the GCE model, the horizontal resolution is usually 2000m with 200 by 200 grid points. The time step is 5 to 10 s. Table 3 lists the characteristics of the GCE model.

3. Applications of the GCE Model to the Study of Precipitation Processes

The application of the GCE model to the study of precipitation processes can be generalized into fourteen categories (Table 4). It has been used to provide essential insights into the interactions of clouds with each other (Tao and Simpson 1984, 1989a), with their surroundings, and their associated heat, moisture, momentum, mass and water budgets (Tao 1978; Soong and Tao 1980, 1984; Tao and Soong 1986; Tao, Simpson and Soong 1987; Tao and Simpson 1989b), with radiative transfer processes (Tao *et al.* 1991, 1993a, 1996; Sui *et al.* 1998), with ocean surfaces (Tao *et al.* 1991; Wang *et al.* 1996, 2000), with idealized climate variations (Lau *et al.* 1993, 1994; Sui *et al.* 1994; Tao *et al.* 1999), and cloud draft structure and trace gas transport (Scala *et al.* 1990; Pickering *et al.* 1992; and a review by Thompson *et al.* 1997) and precipitation efficiency (Ferrier *et al.* 1996). The GCE model has also been used to convert the radiances received by cloud-observing microwave radiometers into predicted rainfall rates (Simpson *et al.* 1988, and a review by Simpson *et al.* 1996). Remote sensing of cloud-top properties by high-flying aircraft bearing microwave and other instruments is now beginning to provide powerful tests of the GCE model, particularly when such observations are augmented by simultaneous ground-based radar measurements (Adler *et al.* 1991; Prasad *et al.* 1995; Yeh *et al.* 1995). The GCE model has also been used to study the distribution of rainfall and inferred heating (Tao *et al.* 1990, 1993b, 2000a and b). In this paper, a brief discussion about the application of the GCE model to **(1)** cloud interaction and mergers, **(2)** convective and stratiform interaction, **(3)** mechanisms of cloud-radiation interaction, **(4)** latent heating profiles and TRMM, and **(5)** responses of deep cloud systems to large-scale processes will be provided. Comparisons between the GCE model's results, other cloud resolving model results and observations will also be examined.

3.1 Cloud Interactions and Mergers

Field experiment data (e.g., FACE, Florida Area Cumulus Experiment; GATE, GARP Atlantic Tropical Experiment; and ITEX, Island Thunderstorm Experiment) has shown that the merging of shower clouds is a crucial factor in the development of organized convective complexes which are the major producers of rainfall in the tropics (Houze and Chang 1977), in the Florida peninsula (Simpson *et al.* 1980) and in the Maritime Continent region north of Darwin, Australia (Simpson *et al.* 1993). The observational data consisted of the calibrated radar and rain gauges. The mergers usually yield more than an order of magnitude more precipitation than unmerged cells. For example, Simpson *et al* . (1980) found that mergers were responsible for 86% of the rainfall observed, even though 90% of the cells were unmerged. Most of the increase in total rainfall comes from the increased areal extent and duration of the second-order mergers. [A first-order merger is identified as a consolidation of two or more previously independent single cell echoes, while a second-order merger is the result of the juncture of two or more first-order merged echoes (Westcott 1984).]

However, the physical mechanisms which effect the merging process are not clearly specified through observational studies, largely because of the difficulty of measuring the air circulations in and around cumulus clouds. Westcott (1984) reviewed observational analyses of mergers in detail, and also raised some key questions concerning the mechanisms involved. From observational studies, several processes have been proposed as important in merging events. These processes fall into two main categories. The first involves addition of moisture to neighboring air, thereby reducing dilution by entrainment (Byers and Braham 1949; Scorer and Ludlam 1953; Malkus 1954). Moistening of the cloud environment can be accomplished in several ways. One source of moisture is precipitation falling from an overhanging canopy which produces a favorable environment for new convective growth. Dissipation of previous and nearby clouds also provides a moister, more favorable environment. The merging cells can be better protected from the entrainment of dry environmental air (Lopez 1978). The second category involves dynamic processes which enhance low-level convergence leading to new growth and merging. Low-level convergence can be enhanced by **(1)** collision of downdraft outflows (Simpson 1980; Simpson *et al.* 1980); **(2)** differential motions of cloud masses (Holle and Maier 1980; Cunning *et al.* 1982; LeMone 1989); and **(3)** hydrostatic and non-hydrostatic pressures response within the boundary layer (Cunning and Demaria 1986; LeMone *et al.* 1988).

3.1.1 The GCE model simulation results

A two-dimensional version of the GCE model was used with a GATE data set to study cloud interactions and merging (Tao and Simpson 1984). Over two hundred groups of cloud systems with a life history of over sixty minutes were generated under the influence of different combinations of the stratification and large-scale forcing (through a total of 48 numerical experiments). The GCE model results demonstrated the increase in convective activity and in amount of precipitation with increased intensity of large-scale forcing (lifting). In the GCE model simulation, a cloud merger is defined as a joining of the surface rainfall contour of 1 mm h^{-1}. Additional criteria are also considered. The merged clouds need to join for at least 15 minutes and the distance between previous separate clouds must be at least four to five grid intervals initially. These conditions are a combination of the definitions of merger found in several observational studies (Changnon 1976; Houze and Change 1977; Simpson *et al.* 1980). Based on the GCE model results, the most unfavorable environmental conditions for cloud merging are 1) less unstable stratification of the atmosphere and 2) weaker large-scale forcing.

One advantage of the model simulations is that the model can be rerun in order to investigate the sensitivity of its results to various physical processes. For example, a pair of runs using identical initial conditions were performed. The only difference is that the drag force of rain water in the vertical equation is set to zero in the sensitivity test. The absence of the drag force can lead to a delay in either the onset or the weakening of the downdraft below the cloud. The new convective cell in the merged situation did not occur in the run with weaker downdrafts. This sensitivity test demonstrated the importance of downdrafts on merger,

Later, a total of nine three-dimensional experiments were made using the same GATE data set (Tao and Simpson 1989a). Ten merged systems involving precipitating clouds were identified. Eight of these ten mergers involved two previously separated clouds (cells E and F); seven of these lie along a line roughly parallel to the initial environmental wind shear vector (called *parallel cells*, see Fig. 1). Only one merger lies along a line roughly perpendicular to the wind shear vector prior to the merging (called *perpendicular cells*, see Fig. 2). The dominance of parallel cells is consistent with observations in FACE and GATE (Simpson *et al.* 1980; Turpeinen 1982). The remaining two systems involve three clouds and are a combination merger of parallel and perpendicular cells. It was also found that a cloud bridge, which consists of a few low-level cumuli which develop and connect the clouds before the merger is detected on radar, occurs in most of the simulated merger cases. (This phenomenon was also well-simulated in the 2-D model.) New cell (Cell G in the parallel merger case and Cell K in the perpendicular meager case) at the cloud bridge area developed vigorously. Both backward and forward air parcel trajectory analyses (Fig. 3) were performed. Forward air parcel trajectories are computed using grid points located in the merging area. Then, a backward trajectory calculation was performed to locate the origins of the high-rising parcels. These trajectory analyses show that the high-rising air parcels at the bridge area originated close to or within the regions occupied by previous separated cells (Cells E and F). These air parcels were strongly affected by either one or two interacting cold outflows. Both 2D and 3D GCE model studies clearly suggest that the primary initiating mechanism for the occurrence of a precipitating cloud merger is the cloud downdrafts and their associated cold outflows as proposed by Simpson (1980). A significant difference between the simulated parallel and perpendicular cells is that the latter cells are usually situated closer to each other (5-6 km) prior to merging, compared to the former (10 km or more). An explanation for this difference is that the direction of individual cell movement as well as the direction of cold outflow are predominantly directed down shear.

3.1.2 Comparison with Other Cloud Resolving Model Results

The causes of merging have been investigated by Hill (1974), Wilkins *et al.* (1976), Orville *et al.* (1980), Turpeinen (1982), Bennetts *et al.* (1982) and Kogan and Shapiro (1996) using cloud resolving models. Orville *et al.* (1980) investigated the effects of varying the spacing, timing and intensity of two initial impulses in the context of a two-dimensional cloud model including warm rain and hail processes. Merging was found to result if two clouds were relatively close to each other (less than 7 km) and if the clouds were of different strength or initiated at different times (at intervals of 6 minutes). The mechanism of merging was attributed to the existence of a pressure gradient directed from the weaker and younger cell toward the older and stronger one. By using a three-dimensional cloud model, Turpeinen (1982) also found that the mechanism of merging was dependent on the perturbation pressure distribution. Note that these two modeling studies used the joining of the 100% relative humidity isopleth of water vapor as a criterion for merger. The formation of a cloud bridge observed by Simpson (1980) has been simulated by both studies. But, vigorous development of the new convective cell at the cloud bridge area did not occur in Orville *et al.* (1980) and Turpeinen (1982). Turpeinen (1982) suggested that this discrepancy might be attributed to the absence of mesoscale convergence in the model simulations.

Kogan and Shapiro (1996) performed three-dimensional numerical simulations of mergers using explicit microphysics in a shear-free environment. Their criterion for cloud merger was based on the visual form of cloud updraft merger on a horizontal cross section. An arbitrary contour interval specified in the graphics routine (2 m/s) for coalescence of vertical velocity was used. This criterion was examined every 300 s. Kogan and Shapiro (1996) found that updraft merger occurred in four of the six simulations. They also found that after updraft merger, the maximum vertical velocity and domain averaged kinetic energy were increased over the single bubble simulation. They hypothesize that the mergers were a consequence of mutual advection, that is each of the clouds advected its neighbor in its radial inflow. Bennetts *et al.* (1982) also attributed merging in their numerical simulations to "mutual attraction". Kogan and Shapiro (1996) also found that the most favorable conditions for merger occur when the cells are closer than 4.5-6 radii apart (about 3-5 km between the centers of the temperature perturbations). No vigorous development occurred after the two updrafts merged, however. No precipitating downdraft was present in their simulations.

There is one major difference between the GCE model simulated mergers and those from others (Orville *et al.* 1980; Turpeinen 1982; Bennetts *et al.* 1982; Kogan and Shapiro 1996). The simulated mergers from other modeling studies are the consolidation of two initial independent single bubbles (the first-order merger). Their simulated mergers do not have vigorous development in contrast to the GCE model simulations. The basic design of the GCE modeling study is to generate several convective clouds randomly inside the model domain and, then, to observe and analyze the interactions between the simulated clouds. Neither locations nor intensities of simulated clouds are predetermined. The mergers identified in Tao and Simpson (1984, 1989a) only involve precipitating clouds (by definition). Their merged cases lasted longer and produced quite significant surface precipitation as observed by Simpson *et al.* (1980, 1993). Tao and Simpson (1989a) found that some of the previously distinct clouds associated with merger cases resulted from the consolidation of smaller-sized clouds. [This may also explain why the mergers discussed in Tao and Simpson (1989a) are very similar to the second-order merged systems observed by Simpson *et al.* (1980).] These smaller sized cells were predominantly oriented along the direction of the wind shear vector when they merged together. This result is inconsistent with the simulation performed by Turpeinen (1982). Situations for this type of merger only involve shallow clouds with little or no surface precipitation. Thus, the mechanism responsible for their merging can not be cloud downdrafts and their associated cold outflows. The pressure distribution, as suggested by Orville *et al.* (1980) and Turpeinen (1982), mutual advection, as suggested by Kogan and Shapiro (1996) and the differential motions between convective elements (LeMone 1989) are probably the major mechanisms for this type of merger. All first-order simulated mergers may require is for two initially separated convective cells to be very close [from 7 km in Orville *et al.* (1982) to about 4 km in Kogan and Shapiro (1996) and Tao and Simpson (1989a)].

The definition of cloud merger is not unique in observational studies (Westcott, 1984). Observational studies are based on radar derived information. The observational studies usually define merger in terms of coalescence of precipitation areas or radar reflectivity (at 1 mm h^{-1}, minimum detectable reflectivity signal). Additional criteria related to the distance between initially distinct convective elements and the duration of precipitation are also sometimes applied. Numerical simulations have used modeled dynamical and thermodynamical parameters (i.e., overlap of buoyancy, updraft, humidity, or circulation fields) to define mergers. Westcott (1984) pointed out that in order to perform better merger studies, it is necessary to clearly relate convective system's dynamical, thermodynamic and microphysical structures and their radar image.

3.2 Convective - Stratiform Interaction

One of the major findings from GATE was the important contribution to rainfall from mesoscale convective systems (MCSs[2]). For example, Houze (1977) estimated that four MCSs accounted for 50% of the rainfall at one of the GATE ships during Phase III. It was also estimated that the widespread stratiform rain accounted for about 32%-49% of the total rainfall from the GATE MCSs (Houze 1977; Zipser *et al.* 1981; Gamache and Houze 1983). In addition, observations indicated that little stratiform rain fell during the early stages of *tropical* MCSs. As the stratiform cloud developed and expanded, the total amount of rain falling from it became equal to that generated in the convective region. The fraction of stratiform rainfall from *midlatitude* squall lines has been estimated at 29%-43% (Rutledge and Houze 1987; Johnson and Hamilton 1988). The existence of unsaturated warm mesoscale descent beneath the stratiform region was identified by Zipser (1969) and conceptualized in Houze (1977) and Zipser (1977). The associated mesoscale ascent at the middle and upper layers of the stratiform region was diagnosed from indirect observations by Gamache and Houze (1983). One type of MCS is a squall line. The conceptual model of tropical and midlatitude squall lines are shown in Fig. 4.

The vertical distribution of heating in the stratiform region of MCSs is also considerably different from the vertical profile of heating in the convective region (Houze 1982; Johnson 1984). The convective profiles always show heating throughout the depth of the troposphere which is maximized in the lowest 2-5 km. The shapes of the heating profiles are quite similar with only slight variations in their magnitude for different MCSs from different geographic locations. The same can generally be said about the stratiform region. Heating is maximized in the upper troposphere, however, between 5 and 9 km while cooling prevails at about 4 km. In addition, many recent studies (Adler and Negri 1988; Tao *et al.* 1993b) indicated that a separation of convective and stratiform clouds is necessary for a successful surface rain and latent heating profile retrieval from remote sensors.

---

2 Houze (1997) defined a mesoscale convective system (MCS) as "a cloud system that occurs in connection with an ensemble of thunderstorms and produces a contiguous precipitation area ~ 100 km or more in horizontal scale in at least one direction".

These findings lead to an important question: *what are the origins and growth mechanisms of particles in stratiform precipitation?* Chen and Zipser (1982) suggested that both depositional growth associated with upward motion in the anvil and the horizontal flux of hydrometeors from the convective region are important in the maintenance of anvil precipitation. In a kinematic model study of a GATE squall line, Gamache and Houze (1983) showed quantitatively that 25-40 percent of the stratiform condensate was created by mesoscale ascent at mid-to-upper levels in the stratiform region itself. Gallus and Johnson (1991) found that the contribution to surface rainfall from condensation in the mesoscale updraft was comparable in magnitude to the transport of condensate rearward from the convective line during a rapidly weakening stage of a mid- latitude squall line. Using a kinematic (steady-state) cloud model, Rutledge (1986) suggested that the condensate produced by mesoscale ascent is largely responsible for the large horizontal extent of light stratiform precipitation to the rear of the same GATE squall line analyzed by Gamache and Houze (1983). Using higher resolution, Doppler-derived air motions associated with a midlatitude squall line as input in their two-dimensional kinematic model, Rutledge and Houze (1987) found that deposition in the mesoscale updraft accounted for 80 percent of the stratiform precipitation. They also conducted a series of sensitivity tests and found that almost no rain reached the surface in the stratiform region without the influx of hydrometeors from the convective cells, while only about one-fourth as much stratiform rain reached the surface in the absence of mesoscale ascent.

3.2.1 The GCE Model Simulations Results

Observational studies have had to use a steady state assumption to estimate the transfer of hydrometeors from the convective region to its associated stratifrom region as well as a relatively simple 1-D cloud model to estimate the microphysical processes within the convective and stratiform regions. The time-dependent cloud resolving models (Tao *et al.* 1993a; Chin 1994; and Caniaux *et al.* 1994; Tao 1995; and others) have been used to explicitly quantify the origins and growth mechanisms of particles in stratiform precipitation by calculating the water budgets (microphysical processes and transfer processes of hydrometeors between convective and stratiform regions).

Several organized convective systems (EMEX, TOGA COARE, TAMEX and PRESTORM), which occurred in different large-scale environments, have been simulated by the GCE model and the associated water budgets were analyzed (Tao *et al.* 1993a; Tao 1995).

Table 5 compares several characteristics of the large-scale flow (i.e., stability, Richardson number, and precipitable water) in which these convective systems were embedded. The propagation speed of these systems and the references for the GCE model simulations are also listed. The convective available potential energy (CAPE) associated with the tropical convective systems is moderate (from 1400 to 1660 m2 s^{-2}) and smaller than that of the midlatitude system (PRESTORM). The vertical integrated water vapor contents are much higher for the TOGA COARE and EMEX cases compared to the PRESTORM case.

The water budgets in the convective, stratiform, and nonraining regions associated with the TOGA COARE, EMEX, TAMEX and PRESTORM convective systems are shown in Fig. 5. The water budgets are separated into three different layers: lower (surface to 10 ^{o}K level), middle (from 10 K to -10 K) and upper (-10 K to 100 mb). The horizontal transfer of hydrometeors from the convective to the stratiform region occurs mainly in the middle troposphere for the EMEX and TOGA COARE convective systems. By contrast, two thirds of the horizontal transfer of hydrometeors is accomplished in the upper troposphere for the PRESTORM case. This is caused by the strong convective updrafts associated with the PRESTORM case. Also a more vigorous transfer of hydrometeors in the lower troposphere from the stratiform region back into the convective region occurs for the PRESTORM case. This is a consequence of the strong rear inflow simulated for this midlatitude case. For the TAMEX case, the horizontal transfer of hydrometeors can occur in both the middle and upper troposphere. A downward transfer of hydrometeors from the middle to the lower troposphere is a dominant process in the stratiform regions for all four cases. The interaction between the stratiform and non-surface-raining region is less significant than that between the convective and stratiform region.

The contribution to stratiform rain by the convective region has to be quantified by estimating a ratio (**R**), $\mathbf{R}=C_T/(C_T+C_m)$, where C_T is the horizontal transfer of hydrometeors from the convective region into the stratiform region above the 10 ^{o}C level, and C_m is the sum of the net condensation in the stratiform region and in the non-raining region above the 10 ^{o}C level. *A small ratio indicates that the horizontal transfer of hydrometeors from the convective region is a small source of condensate for the stratiform anvil, whereas a ratio near unity indicates that nearly all of the condensate in the stratiform region was transported from the convective region.* All four GCE modeled cases showed large ratios, from 0.33 to 0.82, implying the role of the convective region in the generation of stratiform rainfall can not be neglected[3] (Table 6). The relative importance of the horizontal transfer processes to the stratiform water budget is similar between the initial and the mature stages of the TAMEX, TOGA COARE and EMEX systems, and this is likely due to the fact stratiform clouds developed rapidly. In contrast, during the initial stage of the PRESTORM simulation, nearly all of the condensate in the stratiform region was a result of the horizontal transport from the convective region. As the PRESTORM system matured, the contribution made by the horizontal transport of hydrometeors from the convective region (*i.e.*, the ratio R) decreased, such that the sources of condensate in the stratiform water budget were similar for all of the mature storms. It is hypothesized that during the initial stage of the PRESTORM simulation, much of the condensate transported from the convective region is used to moisten and modify the dry environment at middle and upper levels. Condensation and deposition become increasingly more important with time in the stratiform water budget once the larger-scale environment reaches saturation. This evolution in the stratiform water budget is less obvious in the TAMEX, TOGA COARE and EMEX cases because the environment is much more moist. (Note that the TAMEX, EMEX and TOGA COARE cases have more stratiform rainfall than its PRESTORM counterpart.) The GCE model results also indicated that the similarity in R at the mature stages of all systems is likely to be result of large stratiform regions being present.

3.2.2 Comparison with Observational and Other Cloud Resolving Model Results

Table 7 lists the ratio (R) from observational studies using composite wind and thermodynamic fields for five different GATE MCSs (Leary and Houze 1980; Gamache and Houze 1983), a midlatitude squall line (Gallus and Johnson 1991), and a tropical-continental squall line (Chong and Hauser 1989). For six out of the seven observed cases the ratio is very close to or above 0.50. This implies that the convective region plays a very important role in the generation of stratiform rain. Very good agreement is evident between the ratio at the mature stage of the modeled PRE-STORM squall system and that estimated by Gallus and Johnson (1991). The modeled EMEX and TOGA COARE cases indicate a relatively small contribution (0.37) to stratiform formation from the convective region compared to those determined from the kinematic studies.

---

3 The convective region can also transport the water vapor originally from low troposphere into the stratiform region. Sui *et al.* (1994) indicated that this water vapor transport is the source for stratiform formation (deposition and condensation). Dynamic triggering of the stratiform formation can be gravity waves excited by strong and deep convective cells associated with the convective region.

Table 7 also shows the ratios determined from other CRM results (Chin 1994; Chin *et al.* 1995; Caniaux *et al.* 1994). Very good agreement is evident between the ratio at the mature stage of our modeled EMEX and TOGA COARE squall systems and a tropical squall case simulated by Chin *et al.* (1995). The comparison between our simulated PRE-STORM and other CRM simulated midlatitude cases (Chin 1994; and Caniaux *et al.* 1994), however, is quite different. Caniaux *et al.* (1994) suggested that the smaller contribution from the convective region to stratiform formation compared to observational studies (Chong and Hauser 1989) was due to the inability of convective updrafts to transport condensate to high levels in their two-dimensional simulation, the slower propagation speed and the existence of a transition zone. The very smaller stratiform portion (10%) in the midlatitude case simulated by Chin (1994) is the reason for the higher R. The GCE modeled PRESTORM case has a higher R (0.8) and smaller stratiform portion (14%) at the initial stage.

A direct comparison between these studies and the GCE model studies should be done with caution, because a different spatial resolution and a different definition for the convective-stratiform regions was used. For example, Caniaux *et al.* (1994) had a fixed number of model grid points (50) designated as the convective region. Remaining grid points with surface precipitation comprised the stratiform region. In the GCE model, the convective and stratiform regions are identified using information from surface rainrates first (i.e., Churchill and Houze 1984). Additional criteria are applied which have been included to identify regions where convection may be quite active *aloft* though there is little or no precipitation yet at the surface, such as areas associated with tilted updrafts and *new cells* initiated ahead of organized squall lines (Tao *et al.* 1993, Lang *et al.* 2000). The GCE method was adopted by Chin (1984) and Chin *et al.* (1995). The comparison between the GCE simulated PRE-STORM, TOGA COARE, TAMEX and EMEX cases, however, is consistent because the same type of data set and the same criteria for partitioning the convective and stratiform regions were being used.

3.2.3 The Convective and Stratiform Processes in Large-Scale Models

Molinari and Dudek (1992) and Frank (1993) suggested that the best approach to cumulus parameterization in large-scale scale models (30-120 km horizontal resolution, 150-300 second time steps) appears to be "*to use a scheme that operates simultaneously with and interacts explicitly with the explicit scheme (grid scale microphysical processes)*". They termed such schemes "*hybrid schemes*". The hybrid approach (by separating out the forcing mechanism for the mesoscale component) resolves the "mesoscale" circulations and microphysical processes that directly influence the development of the "stratiform clouds". Cumulus parameterization makes use of steady-state cloud models that interact with grid-scale variables and provide net heating, drying, and condensate associated with "convective cells". The interaction between parameterized and explicitly resolved cloud processes is through the *detrainment* of water vapor and condensate generated from the steady-state cloud model into the "resolved" stratiform clouds.

Recently, GCMs and climate models (i.e., CSU GCM and GISS GCM) allow both a cumulus parameterization scheme and an explicit moisture scheme to be activated simultaneously in the model simulations. The cumulus parameterization scheme is generally used to represent convective precipitation (10 km spatial scale) and the explicit moisture scheme to represent grid-resolvable precipitation such as stratiform/cirrus clouds (100-200 km spatial scale). The CSU GCM has implemented an explicit microphyiscal scheme with ***five*** prognostic variables for the mass of water vapor, cloud water, cloud ice, rain and snow (Fowler *et al.* 1996). The GISS global climate model has added an efficient prognostic cloud water (one species only). Stratiform clouds can be coupled with parameterized convection through detrainment of cloud water and/or cloud ice from the "tops" of cumulus towers or at any level above 550 mb (Del Genio *et al.* 1996).

The explicit interaction between cumulus parameterized and grid-scale resolved microphysics is only one-way in the current large-scale models. Note that some water condensate generated by the stratiform region can be transported into the convective region. In addition, how much (all or partial) and where the (cloud tops or above melting layer) parameterized water condensate should detrain into the explicitly resolved microphysical scheme needs to be addressed. The CRM results can and should be used for improving the cumulus parameterization schemes as well as for understanding the interaction between the cumulus parameterization schemes and the explicit moisture schemes. In the future, CRMs can be used to study the time evolution of each of the water budget terms associated with MCSs in different geographical regions as well as to determine whether any important variations in the evolution of the water budget can be explained in terms of differences in the wind and thermodynamic characteristics of the large-scale environments.

3.3 Mechanisms of Cloud-Radiation Interaction

The interaction between clouds and radiation is two-way. On the one hand, clouds can reflect incoming solar and outgoing long-wave radiation. On the other hand, radiation can enhance or reduce the cloud activity. Gray and Jacobsen (1977) suggested that differential cooling between cloudy and clear regions can enhance cloud activity in the cloudy region. Long-wave radiation cools the stratiform cloud top but warms the stratiform cloud base (Cox and Griffith 1979). As a result, long-wave radiation can destabilize the stratiform cloud layer. Webster and Stephens (1980) also suggested that this destabilization was quite an important process in the light precipitation region during WMONEX. Stephens (1983) further suggested that the effects of radiation on the growth and sublimation rates of ice particles are significant. Particle growth (sublimation) is enhanced (suppressed) in a radiatively cooled (heated) environment. Radiative cooling could also destabilize the large-scale environment (Dudhia 1989). The cloud-radiation interaction can also have major impact on the diurnal variation of precipitation processes over the tropics. For example, the thermodynamic response of clouds to radiative heating [cloud development is reduced by solar heating and enhanced by IR cooling - Kraus (1963); Randall *et al.* (1991)] and the large-scale dynamic response to the radiational differences between cloudy and clear regions (Gray and Jacobson 1977) have been suggested as the mechanisms responsible for the diurnal variation of precipitation over tropical oceans.

3.3.1 The GCE Model Simulated Results

A two-dimensional version of the GCE Model has been used to perform a series of sensitivity tests to identify which is the dominant cloud-radiative forcing mechanism with respect to the organization, structure and precipitation processes for both a tropical (EMEX) and a midlatitude (PRESTORM) mesoscale convective system (Tao *et al.* 1996). Figure 6 shows the schematic diagram demonstrating the impact of cloud-radiation mechanisms on surface precipitation for EMEX and PRESTORM cases. The GCE model results indicated that the dominant process for enhancing the surface precipitation in both the PRE-STORM and EMEX squall cases was the large-scale radiative cooling. However, the overall effect is really to increase the relative humidity and not the CAPE. Because of the high moisture in the tropics, the increase in relative humidity by radiative cooling can have more of an impact on precipitation in the tropical case than in the midlatitude case. The large-scale cooling led to a 36% increase in rainfall for the tropical case. The midlatitude squall line with a higher CAPE and lower humidity environment was only slightly affected (7%) by any of the longwave mechanisms. The GCE model results also indicated that the squall systems' overall (convective and stratiform) precipitation is reduced by turning off the cloud-top cooling and cloud-base warming. Therefore, the cloud-top cooling - cloud-base warming mechanism was not the responsible cloud-radiative mechanism for enhancing the surface precipitation. However, the circulation as well as the microphysical processes were indeed (slightly) enhanced in the stratiform region by the cloud-top cooling and cloud-base warming mechanism for the midlatitude squall case. For both cases, the model results show that the mechanism associated with differential cooling between the clear and cloudy regions may or may not enhance precipitation processes (+5% to -7%, respectively for the EMEX and PRESTORM cases). However, this mechanism is definitely less important than the large-scale longwave radiative cooling.

Solar heating was run from 9 AM to 1 PM LST in both environments and was found to decrease the precipitation by 7% in each case, compared to the runs with longwave radiation only. This result suggests that solar heating may play a significant role in the daytime minimum/nighttime maximum precipitation cycle found over most oceans, as noted in the observational study of Kraus (1963). Sui *et al.* (1998) used the GCE model and performed a 15 day integration to simulate TOGA COARE convective systems. Their simulated diurnal variation of surface rainfall is in reasonable agreement with that determined from radar observations. They also found that modulation of convection by the diurnal change in available water as a function of temperature was responsible for a maximum in rainfall after midnight. This simply implies that the increase (decrease) in surface precipitation associated with IR cooling (solar heating) was mainly due to an increase (decrease) in relative humidity. The GCE model results also showed that the diurnal variation of sea surface temperature only plays a secondary role in diurnal variation in precipitation processes.

3.3.2 Comparison with Other Cloud Resolving Model Results

Table 8 lists the previous modeling studies that have investigated the impact of cloud-radiation interactive processes on various cloud systems. The increments in surface precipitation in Table 8 are normalized against the run without radiative processes. The conclusions associated with cloud-radiation mechanisms for our GCE modeled tropical (EMEX) and mid-latitude (PRESTORM) squall cases are in good agreement with many of these previous modeling studies. For example, Xu and Randall (1995), Miller and Frank (1993) and Fu *et al.* (1995) indicated that the differential cooling between cloudy and clear regions plays only a secondary role in enhancing precipitation processes. Xu and Randall (1995) and Fu *et al.* (1995) suggested that the cloud-top cooling and cloud-base warming destabilization mechanism could be important for prolonging the lifespan of high anvil clouds (around 10 km). Xu and Randall (1995) showed that this direct cloud destibilization does not have any impact on surface precipitation. The modeling studies (Fu *et al.* 1995; Miller and Frank 1993) also indicated that more surface precipitation can be generated in runs with constant clear-air radiative cooling than without. In addition, previous modeling results (Chin 1994; Chin *et al.* 1995; Miller and Frank 1993) indicated that solar radiative processes can reduce precipitation processes. However, the amount of increase or decrease in surface precipitation varies quite significantly among these different modeling studies, but only in regard to the tropical convective systems and not the midlatitude systems. One possible explanation is that large-scale forcing (lifting) was needed in some of these different tropical convective system studies. The imposed lifting varied from 2 cm/s to 14 cm/s in magnitude and was applied continuously or discontinuously in time among the different studies (see Table 8). Using an earlier version of the GCE model (Tao and Simpson 1989b), which included a superimposed large-scale vertical velocity as the main forcing, sensitivity tests using two different large-scale vertical velocities were performed. The results show that the radiative effects on the clouds are quite sensitive to the imposed background ascent (or lifting). The larger the imposed vertical velocity (9-12 cm/s) there is, the lesser the impact of longwave cooling on surface precipitation processes (over 24 h of simulation time). Frank and Miller (1993) also obtained a similar conclusion using a regional scale model. Also note that the larger the imposed vertical velocity, the larger the cloud coverage that was generated.

The physical processes responsible for diurnal precipitation were found to be quite different between the GCE model and other CRM studies. For example, Xu and Randall (1995) found that nocturnal convection has basically a direct result of cloud-radiation interactions, in which solar absorption by clouds stabilized the atmosphere. Their simulated rainfall for both non-interactive and interactive radiation were quite similar, however. Liu and Moncrieff (1998) showed that direct interaction of radiation with organized convection was the major process that determined the diurnal variability of rainfall. Their results indicated that well (less) organized cloud systems can have strong (weak) diurnal variations of rainfall. They also suggested that ice processes are needed. The model set-ups between Sui *et al.* (1998) and Liu and Moncrieff (1998) are quite different, however. In Liu and Moncrieff (1998), the horizontal momentum was relaxed to its initial value that had a strong vertical shear in horizontal wind. On the other hand, the horizontal wind was nudged to time-varying observed values in Sui *et al.* (1998). Consequently, only long-lived squall lines (or fast-moving convective systems) were simulated in Liu and Moncrieff (1998) over the entire simulation. In Sui *et al.* (1998), however, their simulated cloud systems had many different sizes and various life cycles. A more rigorous cloud resolving model inter-comparison involving mechanisms associated with diurnal variation is needed in the future. A good quality controlled long term observational data set that can provide large-scale initial conditions is also required.

3.4 Latent Heating Profiles and TRMM

The GCE model has been used to develop a Convective-Stratiform Heating (CSH) algorithm. The CSH algorithm uses surface precipitation rates, amount of stratiform rain, and information on the type and location of observed cloud systems as input. The CSH algorithm also utilizes a lookup table that consists of convective and stratiform diabatic heating profiles for various types of cloud systems in different geographic locations. These profiles are obtained from GCE model simulations by temporally and spatially averaging the heating distributions in the convective and stratiform regions of the systems, which are then normalized by their total surface rainfall (see Fig. 7). The heating profiles (normalized with surface rainrate) shown in Fig. 7 all have a characteristic shape for the convective and stratiform heating (e.g., Houze, 1982; 1997). These include maximum convective heating in the lower to middle troposphere, maximum stratiform (anvil) heating in the upper troposphere, and regions of stratiform cooling prevailing in the lower troposphere. Also, larger heating aloft in the stratiform region is associated with larger cooling in the lower troposphere. However, some notable differences do exist. For example, the level separating the heating and cooling in the stratiform region (indicating the freezing or melting level) is different for the convective systems simulated by the GCE model and determined by diagnostic budget. The differences in the height of the strafiform region cooling probably reflect differences in melting layer height or the type of convective systems (system has erect updrafts has higher height). The cooling is quite strong near the surface for the African convective system due to a dry boundary layer (Caniaux *et al.* 1994). The latent heating profiles modeled by the GCE and determined kinematically[4] are quite different for the GATE convective system. Nevertheless, there is, perhaps, more similarity than difference in these profiles shown in Fig. 7. This may imply that the look-up table may not need a significant number of heating profiles.

Tao *et al.* (2000a) evaluated the CSH algorithm's performance by retrieving the latent heating profiles associated with three TOGA COARE convective episodes (December 10-17 1992; December 19-27 1992; and February 9-13 1993). The inputs for the CSH algorithm were SSM/I (similar to TMI) and Radar (similar to TRMM PR) derived rainfall and stratiform amount. Diagnostically determined latent heating profiles calculated using 6 hourly soundings were used for validation. The temporal variability of retrieved latent heating profiles using radar estimated rainfall and stratiform amount was in good agreement with that diagnostically determined for all three periods. However, less rainfall and a smaller stratiform percentage estimated by radar resulted in weaker (underestimated) latent heating profiles and lower

---

4 The convective and stratiform heating profiles were derived using composite "kinematic and thermodynamic" fields from radar, upper air soundings and aircraft measured winds.

maximum latent heating levels compared to those determined diagnostically. Rainfall information from SSM/I can not retrieve individual convective events due to poor temporal sampling. Nevertheless, this study suggested that a good rainfall retrieval from SSM/I for a convective event can lead to a good latent heating retrieval.

The four-dimensional latent heating structure over the global tropics for February 1998 was obtained using TRMM rain products in Tao *et al.* (2000b). Figure 8 shows monthly (February 1998) mean latent heating at three different altitudes (2, 5 and 8 km) over the global tropics from the CSH algorithm. The horizontal distributions or patterns of latent heat release identify the areas of major convective activity (i.e., a well defined ITCZ in the Pacific, a distinct SPCZ) in the global tropics. A well defined ITCZ in the east and central Pacific and in the Atlantic Ocean, a distinct S. Pacific Convergence Zone (SPCZ), and broad areas of precipitation events spread over the continental regions, are present. Also, stronger latent heat release (10 K/day or greater) in the middle and upper troposphere is always associated with heavier surface precipitation. Heating in the upper troposphere over the Pacific and Indian Oceans is much stronger than the heating over Africa, S. America and the Atlantic Ocean. The difference in retrieved convective and stratiform properties between the various geographic locations is the major reason for the difference in the heights of the maximum latent heating level. Higher stratiform amounts always contribute to higher maximum latent heating levels. Whether the higher stratiform proportions and more frequent vigorous convective events in the Pacific are related to the warmer SSTs needs to be studied using multi-season and multi-year retrieved latent heating profiles. Note that differential heating between land and ocean in the upper troposphere could generate strong horizontal gradients in the thermodynamic fields and interact with the global circulation.

One interesting result from Fig. 8 is the relatively strong cooling (-1 to -2 K/day) at 2 km over the (East, Central and South) Pacific and Indian Oceans but not over the continental regions (i.e., Africa and S. America). This result is due to the fact that the TMI observations had less stratiform precipitation over the continental regions which is not conducive to retrieving stronger low level cooling over the continental regions relative to the tropical oceans. However, it is still not an expected result because the moisture content is higher over oceans. Cooling by evaporation of raindrops in the lower troposphere should be stronger over dry areas. Several previous observational studies were performed to analyze the heating budget obtained from sounding networks over the Pacific warm pool region and the Amazon region. For example, Lin and Johnson (1996) found weak cooling at low levels, probably induced by mesoscale downdrafts or evaporation by shallow cumuli, in the mean heating profile over the

TOGA COARE region for the month of February 1993. Greco *et al.* (1994) calculated latent heating profiles from the ABLE network. Their results indicated that the distribution of heating is quite similar to the studies of those of West African squall lines (Chong and Hauser 1990). Peak heating occurs between 500 and 550 hPa (about 5-6 km). Their results did not exhibit low level diabatic cooling for the ABLE case. They suggested that the lowermost 2-3 km over the Amazon rain forest canopy is characterized by a strong diurnal cycle of evapotranspiration and upward convective fluxes of moisture producing very large mixing ratios (Fitzjarrald *et al.* 1990). Model results (Scala *et al.* 1990) also suggested that dry tropospheric air is not present for the production and maintenance of evaporatively cooled downdrafts. The high moisture content during the wet season in the lower troposphere of the Amazon Basin may prevent or severely limit cooling below cloud base. Thus, more low level cooling over the Pacific than over S. America as estimated by the CSH heating algorithm is, perhaps, reasonable.

The CSH algorithm estimated heating profiles show one maximum heating level, and the level varies between convective activity from various geographic locations. These features are in good agreement with the heating profiles obtained from the results of diagnostic studies over a broad range of geographic locations (Yanai *et al.* 1973; Johnson 1984, 1992; Thompson *et al.* 1979; Houze 1989; Frank and McBride 1989; Greco *et al.* 1994; Frank *et al.* 1996; Lin and Johnson 1996 and many others). The magnitude of their estimated latent heating release is also in good agreement with those determined from diagnostic budget studies.

Two other latent heating retrieval algorithms, the Goddard Profiling (GPROF) heating, and the Hydrometeor heating (HH), were also used to estimate the latent heating for February 1998 and their results were compared to the those estimated by the CSH algorithm. The horizontal distribution or patterns of latent heat release from the three different heating retrieval methods are quite similar. They all can identify the areas of major convective activity [i.e., a well defined Intertropical Convergence Zone (ITCZ) in the Pacific, a distinct SPCZ] in the global tropics. The magnitude of their estimated latent heating release is also in good agreement with each other and with those determined from diagnostic budget studies. However, the major difference among these three heating retrieval algorithms is the altitude of the maximum heating level. The CSH algorithm estimated heating profiles only show one maximum heating level, and the level varies between convective activity from various geographic locations. These features are in good agreement with diagnostic budget studies. By contrast, a broader maximum of heating, often with two embedded peaks, is generally derived from applications of the GPROF heating and HH algorithms, and the response of the heating profiles to convective activity is less pronounced. Also, GPROF and HH generally yield heating profiles with a maximum at somewhat lower altitudes than CSH.

Heating profiles for the TRMM Field Campaign sites (i.e., SCSMEX, May - June 1998; LBA - TRMM/Brazil, January - February 1999; and KWAJEX, July - September 1999) as well as other major field campaigns such as DOE/ARM will be produced using the three different heating algorithms, and these will be compared to profiles determined from the field campaign sounding networks. This future comparison can provide an assessment of the absolute and relative errors of the heating retrieval algorithms. In addition, global analyses will be used to identify/compare the large-scale circulation patterns for the retrieved periods and for periods during previous field campaigns (i.e., TOGA COARE and GATE). It is reasonable to assume that the latent heating structures for Westerly Wind Bursts (WWBs) and Super Cloud Clusters (SCCs) occurring in similar large-scale circulations and with similar SSTs may not be very different.

3. 5 Response of Tropical Deep Cloud Systems to Large-Scale Processes

Generally speaking, the role of clouds in the atmospheric general circulation and global climate is two-fold. On the one hand, clouds owe their origin to large-scale dynamical forcing, radiative cooling in the atmosphere and turbulent transfer processes between the ground and the atmosphere (e.g., the transfer of heat and moisture from the ocean to the atmosphere). On the other hand, the latent heat from precipitating clouds provides most of the energy received by the atmosphere. Clouds also serve as important mechanisms for the vertical re-distribution of momentum, trace gases (including Greenhouse gas, CO_2) and sensible and latent heat on the large-scale. They also influence the coupling between the atmosphere and the earth's surface as well as the radiative and dynamical-hydrological balance.

The use of cloud resolving models (CRMs) in the study of tropical convection and its relation to the large-scale environment can be generally categorized into two groups. The first approach is so-called "*cloud ensemble modeling*". In this approach, many clouds of different sizes in various stages of their lifecycles can be present at any model simulation time. The large-scale effects which are derived from observations are imposed into the models as the main forcing, however. In addition, the cloud ensemble models use cyclic lateral boundary conditions (to avoid reflection of gravity waves) and require a large horizontal domain (to allow for the existence of an ensemble of clouds). The clouds simulated from this approach could be termed "*continuous large-scale forced convection*". This approach is always applied for simulation associated with tropical deep convection. On the other hand, the second approach for cloud resolving models does require large-scale effects to initialize the clouds. This type of approach usually requires initial temperature and water vapor profiles which have a medium to large CAPE, and an open lateral boundary condition is used. The modeled clouds, then, are initialized with either a cool pool, warm bubble or surface processes (i.e., land/ocean fluxes). These modeled clouds could be termed "*self-forced convection*". The key developments in the cloud ensemble modeling using the continuous large-scale forced convection approach over the past two decades were listed in Table 2.

3.5.1 Simulated Results from the GCE Model

Tao *et al.* (1987) used 2-D and 3-D versions of the GCE model to study the statistical properties of cloud ensembles for a well-organized intertropical convergence zone (ITCZ) rainband that occurred during GATE. The statistical properties of clouds, such as mass flux by cloud drafts and vertical velocity as well as condensation and evaporation were examined. Figure 9 shows heating rates by condensation (c) and evaporation (e) in the 2-D model and the 3-D model. The heating rate estimated from large-scale observations, Q_1[5] - Q_R, and the total cloud heating rate in the 3-D model are also included. The rate of condensation in the 3-D case is slightly larger than its 2-D counterpart, but so is the rate of evaporation. As a consequence, the net heating effect of clouds in the 3-D model is nearly equal to the 2-D counterpart, and both agree with Q_1 - Q_R as estimated from the large-scale heat budget. The GCE model also found that the 3-D modeled surface rainfall rates have smaller standard deviation than their 2-D counterparts. Overall, the GCE model results indicated that collective thermodynamic feedback effects and vertical transports of mass, sensible heat and moisture by the convective cells show profound similarities between the two- and three-dimensional GCE model simulations.

Zipser and LeMone (1980) and LeMone and Zipser (1980) presented the results of statistical analyses of convective updrafts and downdrafts. Their analyses were based on aircraft data gathered from cumulonimbus cloud penetrations for six days during GATE. In order to facilitate a comparison between our model results and their analysis results, we subdivided the updrafts and downdrafts into active or inactive updrafts and downdrafts (Table 9). For example, a grid point in the model is designated as an active updraft region if (a) the total liquid water content exceeds 0.01 g kg^{-1} and (b) the vertical velocity is larger than 1 m s^{-1} (or 2 m s^{-1}, depending upon how we define "active") at that grid point and at that integration time. These ratios between active cloud updrafts and downdrafts indicate an excellent agreement among results from the 2-D and 3-D models as well as the cores as measured by Zipser and LeMone (1980). Both 2-D and 3-D model results also showed a similar feature in

5 Q_1 is the apparent heat source budget defined in Yanai *et al.* (1973).

that the active updrafts account for approximately 75% of the upward mass flux due to clouds and yet they only cover about 12-14% of the total area. This result is consistent with the concept, first proposed by Riehl and Malkus (1958; see also Riehl and Simpson 1979), that hot towers play a critical role in the heat and moisture budgets in the tropics, even though they occupy a small fraction of the area. Overall, our comparison study has indicated that the statistical properties of the clouds obtained in the 2-D model are essentially the same as the 3-D counterpart given an identical large-scale environment (see Tao 1983). The explanation for this similarity between the 2D and 3D simulations is that the same large-scale advective forcing in temperature and water was superimposed into the GCE model as the main forcing. The cyclic lateral boundary condition used in the GCE model does not allow for additional forcing in the model domain. A two-dimensional simulation should, therefore, give a good approximation of the continuous large-scale forced convection.

Large-scale models (i.e., general circulation and climate models) require not only the global surface rainfall pattern but also the associated vertical distribution within the Q_1 and Q_2[6] budgets. The GCE model can help to identify which processes should be parameterized by the large-scale model, as well as provide information on the vertical profiles of the Q_1 and Q_2 budgets (Tao 1978; Soong and Tao 1980; Tao and Soong 1986; Tao *et al.* 1993a and many others). The GCE model was used to examine the Q_1 and Q_2 budgets of various cloud systems that developed in different geographic locations (GATE, EMEX, PRESTORM, TOGA COARE, ABLE, TAMEX and others). In all of these simulations, the heating due to the vertical eddy convergence/divergence term in sensible heat by convective clouds is always one order of magnitude smaller than that produced by condensation at most levels [Fig. 10(a)]. On the other hand, the maximum value of the cooling rate by evaporation is more than half of the heating rate by condensation. This finding implies that the sum of the condensation and evaporation would provide a good approximation to the total cloud heating rate. The cloud heating effect would be considerably overestimated if heating by condensation alone is considered, ignoring cooling by evaporation. For the Q_2 budget, the GCE model results indicated that the net vertical eddy convergence/divergence of moisture by clouds is generally smaller than the rate of condensation or evaporation, but it is not negligible [Fig. 10(b)]. The different roles of the vertical eddy convergence/divergence term in the Q_1 (temperature) and Q_2 (water vapor) budgets is the major reason for Q_1 and Q_2 decoupling (the level of maximum values in the Q_1 and Q_2 profiles is not at the same level). The GCE model generated heating and drying effects agree well with those estimated from observations.

---

6 Q_2 is the apparent moisture sink budget defined in Yanai *et al.* (1973).

GATE (1974 - in the East Atlantic) and TOGA COARE (1992-1993 - in the West Pacific warm pool region) are perhaps two of the best planned and well coordinated field campaigns for understanding tropical convective systems and their interactions with the large-scale environments within which they are embedded. An improved GCE model (ice microphysics, cloud-radiation interaction, dynamics. and surface fluxes) was used to study the response of convective systems to the large-scale environment using the data collected during GATE and TOGA COARE. The GCE model was integrated for 7 and 8 days, respectively, for GATE (September 1 to 8, 1974) and TOGA COARE (December 19 to 27, 1992). Both runs used 1024 horizontal grid points with a 1 km resolution and 41 vertical grid points with varying resolution (40 m near the surface to 1000 m at the top level). The time step was 7.5 s.

The large-scale environments associated with the organized cloud systems that occurred in TOGA COARE and GATE were quite different. The large-scale advective forcing in temperature and water vapor as well as the large-scale vertical velocity are stronger for TOGA COARE than for GATE. The large-scale vertical velocity shows a diurnal signature in TOGA COARE but not in GATE. The mean CAPE is larger in GATE than in TOGA COARE. The SST is higher for TOGA COARE (about 29 ^{o}C vs 27.4 ^{o}C for GATE). The vertically integrated water vapor content (precipitable water) is much drier for GATE (2.47 g cm^{-2}) than TOGA COARE (5.15 g cm^{-2}). The mean vertical shear from the surface to 700 mb of the large-scale horizontal wind is slightly larger for GATE than TOGA COARE during the GCE model simulation periods. However, the shear is much stronger from over the entire depth of the troposphere in TOGA COARE. The low-level wind shear can determine the organization of convective systems.

Figures 11 (a) and (b) show the temporal variation of the GCE model simulated domain mean surface rain rate for TOGA COARE and GATE, respectively, There are more convective systems simulated by the GCE model for TOGA COARE than for GATE. This is due to the stronger large-scale forcing imposed in the TOGA COARE simulation. The model simulated surface precipitation showed a very complex structure for TOGA COARE compared with GATE. Overall, the GCE model-simulated cloud systems propagated in one direction while the individual cells embedded within the systems propagated in the opposite direction. In addition, the cloud tops propagate in the opposite direction of the associated surface precipitation. These two hierarchies of convection organization are in good agreement with other modeling studies (Wu *et al.* 1998) and with satellite observations (Nakazawa 1988; Sui and Lau 1989). In the GATE simulation, only shallow convective systems developed during the first day. Then, deep convective clouds and non-squall (slow moving) cloud systems developed and propagated westward with the mean wind. Squall line type (fast moving) cloud systems developed after September 4. After September 6, the systems simulated by the GCE model were less organized and produced less surface precipitation compared to the non-squall and squall systems. These GCE model simulated GATE features are in good agreement with other modeling studies (Grabowski *et al.* 1996; Xu and Randall 1996) and observations.

The GCE model simulated domain averaged surface rainfall (mm), and stratiform amount (percentage) for both TOGA COARE and GATE are shown in Table 10. The ratios between evaporation and condensation, sublimation and deposition, and deposition and condensation were examined for both cases. These ratios illustrate the relative importance of warm verse ice processes and source and sink terms associated with water vapor over the course of the TOGA COARE and GATE simulations. The microphysical processes are broken down according to convective organization (i.e., slow-moving, fast-moving, less organized convective episodes from GATE, vigorous deep convection and weaker convective events during the Westerly Wind Burst period) in Table 3.5.2. As expected, more surface rainfall was simulated by the GCE model for TOGA COARE (153.9 mm) than for GATE (91.46 mm). Also, a higher stratiform component was simulated for TOGA COARE (45%) than for GATE (32%). The surface rainfall and stratiform component simulated by the GCE model for TOGA COARE are in reasonable agreement with the rainfall determined from soundings and the stratiform amount measured by radar [see Tao et al. (2000a) for a detailed comparison]. This close agreement is mainly caused by the fact that the GCE model was forced by large-scale tendencies in temperature and water vapor that were derived from the sounding network. However, the GCE model simulated surface rainfall is almost twice that estimated by radar. Johnson and Ciesielski (2000) indicated that the ship radars were located within a relatively dry region of the IFA. The lower rainfall estimates from the ship radars could also be caused by the specific Z-R relationship applied in Short et al. (1997). Based on radar observations (Houze 1997), the GCE model may have underestimated the stratiform rain for GATE fast-moving squall systems. The dominance of warm rain processes in the GATE squall and non-squall convective systems may explain the smaller stratiform rain amounts simulated by the GCE model. Very little ice processes on September 6 and 8 are an indication of shallower convection. In contrast, ice processes are quite important for both active and relatively inactive convective periods during TOGA COARE. Even though the large-scale environment is drier for GATE than TOGA COARE, evaporation is only 54% of the condensation in GATE compared to 71% in TOGA COARE. Weak convective episodes in both GATE and TOGA COARE had high ratios between evaporation and condensation compared to more intense convective periods. The ratio of sublimation to deposition was smaller in the GATE simulation.

3.5.2 Comparison with Other Cloud Resolving Model Results

Krueger (1988) developed a two-dimensional cloud model with a third-moment turbulence closure for simulating an ensemble of cumulus clouds. He simulated the response of cumulus clouds to large-scale forcing, under large-scale conditions observed during GATE. Krueger (1988) found that cloud-scale vertical transport of moisture and evaporative cooling are significant in the Q_2 and Q_1 budgets, respectively. The cloud scale vertical advection of heat is only important in the subcloud layer in the Q_1 budget. These results are consistent with our GCE model simulations. Lafore and Redelsperger (1991) applied a two-dimensional cloud model to simulate a fast moving Tropical squall line observed during COPT81 and a frontal system observed during European MFDP/FRONTS87. Their results also indicated the importance of evaporative cooling and cloud transport of moisture for these two cases. Furthermore, their results showed a relatively small effect by cloud transport of heat on the Q_1 budget except near the subcloud layer. The different roles of the vertical eddy convergence/divergence term in the Q_1 (temperature) and Q_2 (water vapor) budgets is also the major reason for Q_1 and Q_2 decoupling in both systems as indicated by Lafore and Redelsperger (1991).

Grabowski *et al.* (1998) examined the effects of resolution and the third spatial dimension for cloud systems observed during Phase III of GATE (September 1 to 7, 1974). Xu and Randall (1996) used the two-dimensional model developed by Krueger (1988) to simulate cloud systems observed during Phase III of GATE (September 1 to 18, 1974). Wu *et al.* (1998) also used a two-dimensional model to examine the cloud properties associated with cloud systems observed during TOGA COARE (December 5 1992 to January 12 1993). Donner *et al.* (1999) used a three-dimensional model developed by Lipps and Helmer (1986) to simulate several GATE convective systems. The major difference for these modeling studies (and the improved GCE model simulation shown in Fig. 11) from the previous CRM simulations is that they performed long term integrations. All these studies' simulated Q_1 and Q_2 budgets are in good agreement with observations. This is due to the fact that the observed large-scale advective forcing in temperature and water vapor were imposed as suggested by Soong and Tao (1980). Cloud organization in both studies also agreed well with observations due to the fact that the modeled simulated horizontal wind was relaxed to the observed time varying large-scale horizontal wind. The importance of vertical shear of the large-scale horizontal wind on the organization of tropical convective systems was recognized in theoretical studies (i.e., Moncrieff 1992) and numerical simulations (Tao and Soong 1986; Dudhia *et al.* 1987).

Larger temporal variability in the two-dimensional integration than in the three-dimensional integration was found in Grabowski *et al.* (1998) and Donner *et al.* (1999). Donner *et al.* (1999) suggested that this is probably related to the different behavior of the CAPE and convective inhibition (CIN) in two and three dimensions. Grabowski *et al.* (1998), however, concluded that, as long as high-frequency temporal variability is not of primary importance, low-resolution two-dimensional simulations can be used as realizations of tropical cloud systems for addressing the climate problem and for improving and testing cloud parameterizations for large-scale models. This conclusion is only valid for CRMs using large-scale advective forcing and applied with periodic lateral boundary conditions. A similar conclusion was also obtained the results of the GCE model.

However, there are several notable differences between two- and three-dimensional CRM simulations. For example, a weaker convective updraft and a stronger convective downdraft velocity were simulated for a GATE fast moving system in the GCE two-dimensional model compared with in the three dimensional model. Yet, the total upward and downward mass fluxes are almost identical between the two- and three-dimensional GCE model simulations. Lipps and Helmer (1986), however, found that their two-dimensional model had stronger upward and downward mass fluxes than their three-dimensional counterpart for the same GATE simulation as Tao and Soong (1986). They also found more evaporation of cloud water in the two dimensional simulation and consequently less cloud water was present. These results are very different from those of Wu and Moncrieff (1998) for simulations of TOGA COARE convective systems. More ice water and liquid water were simulated in the two-dimensional model than the three-dimensional model in Wu and Moncrieff (1998). The different cases simulated between Lipps and Helmer (1986) and Wu and Moncrieff (1998) is, perhaps, one of the major reasons for the differences. The microphysical schemes used in these two studies are also different. More detailed comparisons are needed in future. The GCSS model intercomparison project and field campaigns (ARM, TRMM LBA, TWAJEX and NASA CAMEX[7]) can provide good quality observational data sets for CRM initialization as well as for its validation.

---

7 ARM stand for Atmospheric Radiation Measurement, LBA for Large Scale Biosphere-Atmosphere Experiment, SCSMEX for South China Sea Monsoon Experiment, KWAJEX

4. Future developments and works

There is much more work to be done comparing simulated cloud systems over various types of land and vegetation environments, ranging from arid to jungle. Recently completed field programs (TOGA-COARE, ARM, TRMM LBA, TRMM KWAJEX and NASA CAMEX) should provide a good opportunity to orchestrate combined observational and numerical studies of convective systems. These large-scale field campaigns can provide some of the desperately needed observations for key locations. These observations can guide and correct existing microphysical schemes used in the CRMs.

Recently, physical processes represented in the spectral bin-microphysical scheme has been implemented into the two-dimensional version of the GCE model. The formulation of the microphysical processes is based on solving stochastic kinetic equations for the size distribution functions of water droplets (cloud droplets and raindrops), and six types of ice particles: ice crystals (columnar, plate-like and dendrites), snowflakes, graupel and frozen drops. Each type is described by a special size distribution function containing 43 categories (bins). The bulk density is equal to 0.9 g cm^{-3} for ice crystals. Snowflakes, graupel and frozen drops are assumed to be spheres and their densities range from 0.01 g cm^{-3} to 0.9 g cm^{-3}. The terminal fall velocities used are those applied by Khain and Sednev (1995), List and Schemenauer (1971) and Cotton *et al.* (1986). Nucleation (activation) processes are based on the size distribution function for cloud condensation nuclei (43 size categories). The GCE model using the spectral bin-microphysics can be used to study cloud-aerosol interactions and nucleation scavenging of aerosols, as well as the impact of different concentrations and size distributions of aerosol particles upon cloud formation. These findings will, in turn, be used to improve the bulk parameterizations. With the improved GCE model, it is expected to lead to a better understanding of the mechanisms that determine the intensity and the formation of precipitation for a wide spectrum of atmospheric phenomenon (i.e., clean or dirty environment) related to clouds.

In addition, cloud microphysical processes, heat fluxes from the warm ocean, land and radiative transfer processes should interact with each other. How these processes interact under different environmental conditions should be a main focus of modeling studies in the

---

for The Kwajalein Experiment, CAMEX for Convection and Moisture Experiment, and TEFLUN for TExas/FLorida UNderflights Experiment future. Also, a major area of needed development involves scale interactions and how cloud processes must be included in simulations of mesoscale to global-scale circulation models. Specifically, Moncrieff and Tao (1999) suggested that improved CRMs can be used to addresses the following aspects in the near future:

1. Derive physically based parameterizations for numerical weather prediction models and climate models;
2. test single-column representations of physical processes (i.e., the processes that trigger convection, cloudiness and convective momentum transport);
3. complement large-scale field experiments that would otherwise be subcritical in terms of cloud-scale measurements;
4. add value to data sets in situations where standard soundings are the only measurement available;
5. improve the physical basis of surface (land and ocean)-atmosphere interaction in coupled climate models;
6. help in the design of space-based and earth-based remote sensing and in the interpretation of the data sets; and
7. understand the vortex formation that may be important for initial tropical cyclone (hurricane) development.

Since the real atmosphere is three-dimensional, three-dimensional cloud resolution model simulations are also needed to address the above scientific problems.

5. Acknowledgments

The work presented in this paper was done collectively by many members of the mesoscale modeling group in the Mesoscale Atmospheric Processes Branch, Dr. W. Lau's group in the Climate Radiation Branch, and Drs. A. Thompson and K. Pickering in the Atmospheric Chemistry and Dynamics Branch at NASA/Goddard Space Flight Center. The author appreciates the inspiring and enthusiastic support by his mentor, Dr. Joanne Simpson, over the past 18 years. Dr. J. Simpson has also set-up a good example for the author to follow. due to her high expectations in doing quality research and publications. She also taught the author to appreciate the art of observational works. The author also thanks Mr. S. Lang for reading the manuscript and Drs. R. Adler and F. Einaudi of NASA/Goddard Space Flight Center for their support.

The author is also grateful to Dr. R. Kakar at NASA headquarters for his continuous support of this research. In addition, Drs. J. Theon and J. Dodge are acknowledged for their early support of Goddard Cumulus Ensemble model improvements and applications. The work is mainly supported by the NASA Headquarters Physical Climate Program and the NASA Tropical Rainfall Measuring Mission (TRMM). Acknowledgment is also made to the NASA/Goddard Space Flight Center for computer time used in this research.

6. References

Adler, R. F., and A. J. Negri, 1988: A satellite infrared technique to estimate tropical convective and stratiform rainfall. *J. Appl. Meteor.*, **27**, 30-51.

Adler, R. F., H.-Y. Yeh, N. Prasad, W.-K. Tao and J. Simpson, 1991: Microwave rainfall simulations of a tropical convective system with a three-dimensional cloud model. *J. Appl. Meteor.*, **30**, 924-953.

Auer, A. H., Jr., and J. D. Marwitz, 1968: Estimates of air and moisture flux into hailstorms on the High Plains. *J. Appl. Meteor.*, **7**, 196-198.

Baker, R. D., B. H. Lynn, A. Boone and W.-K. Tao, 2000: The influence of soil moisture, coastline curvature, and the land-breeze circulation on sea-breeze initiated precipitation, *J. of Hydrometeorology*, (in revision).

Bennetts, D. A., M. J. Bader, and R. H. Marles, 1982: Convective cloud merging and its effect on rainfall. *Nature*, **300**, 42-45.

Braham, R. R., Jr., 1952: The water and energy budgets of the thunderstorm and their relation to thunderstorm development. *J. Meteor.*, **9**, 227-242.

Byers, H. R., and R. R. Braham, Jr., 1949: The Thunderstorm: Report of the Thunderstorm Project. U. S. Government Printing Office, 287pp.

Caniaux, G., J.-L. Redelsperger, and J.-P. Lafore, 1994: A numerical study of the stratiform region of a fast-moving squall line. Part I: General description and water and heat budgets. *J. Atmos. Sci.*, **51**, 2046-2074.

Changnon, S. A.. Jr., 1976: Effects of urban areas and echo merging on radar echo behavior, *J. Appl. Meteor.*, **15**, 561-570.

Chen, S., and W. R. Cotton, 1988: The sensitivity of a simulated extra-tropical mesoscale convective system to longwave radiation and ice-phase microphysics. *J. Atmos. Sci.*, **45**, 3897-3910.

Chen, Y.-L., and E. J. Zipser, 1982: The role of horizontal advection of hydrometeors in the water budget of a large squall system. *Preprints, 12th Conf. on Severe Local Storms*, San Antonio, Amer. Meteor. Soc., 355-358.

Chin, H.-N. S., 1994: The impact of the ice phase and radiation on a mid-latitude squall line system. *J. Atmos. Sci.*, **51**, 3320-3343.

Chin, H.-N. S., Q. Fu, M. M. Bradley, and C. R. Molenkamp, 1995: Modeling of a tropical squall line in two dimensions and its sensitivity to environmental winds and radiation. *J. Atmos. Sci.*, **52**, 3172-3193.

Chong, M., and D. Hauser, 1989: A tropical squall line observed during the COPT 81 experiment in west Africa. Part II: Water budget. *Mon. Wea. Rev.*, **117**, 728-744.

Chong, M. and D. Hauser, 1990: A tropical squall line observed during the COPT 81 experiment in West Africa. Part III: Heat and moisture budgets. *Mon. Wea. Rev.*, **118**, 1696-1706.

Chou, M.-D., 1990: Parameterization for the absorption of solar radiation by O_2 and CO_2 with application to climate studies. *J. Climate*, **3**, 209-217.

Chou, M.-D., 1992: A solar radiation model for use in climate studies. *J. Atmos. Sci.*, **49**, 762-772.

Chou, M.-D., and M. J. Suarez, 1994: An efficient thermal infrared radiation parameterization for use in general circulation models. NASA Tech. Memo. 104606, **3** , 85 pp.

Chou, M.-D., A. Arking, J. Otterman, and W. L. Ridgway, 1995: The effect of clouds on atmospheric absorption of solar radiation. *Geophy. Res. Lett.*, **22**, 1885-1888.

Churchill, D. D., and R. A. Houze, Jr., 1984: Development and structure of winter monsoon cloud clusters on 10 December 1978. *J. Atmos. Sci.*, **41**, 933-960.

Churchill, D. D., and R. A. Houze, Jr., 1991: Effects of radiation and turbulence on the diabatic heating and water budget of the stratiform region of a tropical cloud cluster. *J. Atmos. Sci.*, **48**, 903-922.

Clark, T. L., 1979: Numerical simulations with a three-dimensional cloud model: lateral boundary condition experiments and multicellular severe storm simulations. *J. Atmos. Sci.*, **36**, 2191-2215.

Cotton, W. R., and G. J. Tripoli, 1978: Cumulus convection in shear flow - three-dimensional numerical experiments. *J. Atmos. Sci.*, **35**, 1503-1521.

Cotton, W. R., G. J. Tropoli, R. M. Rauber, E. A. Mulvihill, 1986: Numerical simulation of the effect of varying ice crystal nucleation rates and aggregation processes on orographic snowfall. *J. Appli Meteor.*, **25**, 1658-1679.

Cox, S. K., and K. T. Griffith, 1979: Estimates of radiative divergence during Phase III of the GARP Atlantic Tropical Experiment: Part II. Analysis of Phase III results. *J. Atmos. Sci.*, **36**, 586-601.

Cunning, J. B., R. L. Holle, P. T. Gannnon and A. I. Watson, 1982: Convective evolution and merger in the FACE experiment area: mesoscale convection and boundary layer interaction. *J. Appl. Meteor.*, **21**, 953-977.

Cunning, J. B., and M. DeMaria, 1986: An investigation of the development of cumulonimbus systems over South Florida. Part I: Boundary layer interactions. *Mon. Wea. Rev.*, **114**, 5-24.

Del Genio, A. D., M.-S. Yao, W. Kovari and K. K.-W. Lo, 1996: A prognostic cloud water parameterization for global climate models. *J. Climate*, **9**, 270-304.

Dharssi, I., R. Kershaw, and W.-K. Tao, 1996: Longwave radiative forcing of a simulated tropical squall line. *Quart. J. Roy. Meteor. Soc.,* **123**, 187-206, 1997.

Donner, L. J., C. J. Seman abd R. S. Hemler, 1999: Three-dimensional cloud-system modeling of GATE convection, *J. Atmos. Sci.*, **56**, 1885-1912.

Dudhia, J., 1989: Numerical study of convection observed during the Winter Monsoon Experiment using a mesoscale two-dimensional model. *J. Atmos. Sci.*, **46**, 3077-3107.

Dudhia, J., M. W. Moncrieff and D. W. K. So, 1987: The two-dimensional dynamics of west African squall lines. *Quart. J. Roy. Meteor. Soc.*, **113**, 567-582.

Ferrier, B. S., 1994: A double-moment multiple-phase four-class bulk ice scheme. Part I: Description. *J. Atmos. Sci.*, **51**, 249-280.

Ferrier, B. S., W.-K. Tao, and J. Simpson, 1995: A double-moment multiple-phase four-class bulk ice scheme. Part II: Simulations of convective storms in different large-scale environments and comparisons with other bulk parameterizations. *J. Atmos. Sci.*, **52**, 1001-1033.

Ferrier, B. S., J. Simpson and W.-K. Tao, 1996: Factors responsible for different precipitation efficiencies between midlatitude and tropical squall simulations. *Mon. Wea. Rev.*. **124**, 2100-2125.

Fitzjarrad, D. R., K. E. Moore, O. M. R. Cabral, J. Scala, A. O. Manzi and L. D. de Abreu, 1990: Daytime turbulent exchange between the Amazon forest and the atmosphere. *J. Geophys. Res.*, **95**, 16825-16838.

Fowler, L. D., and D. A. Randall, 1996: Liquid and ice cloud microphysics in the CSU general circulation model. Part I: Model description and simulated microphysical processes. *J. of Climate*, **9**, 489-529.

Frank, W. M., and J. L. M. Bride, 1989: The vertical distribution of heating in AMEX and GATE cloud clusters. *J. Atmos. Sci.*, **46**, 3464-3478.

Frank, W. M., H. Wang, and J. L. McBride, 1996: Rawinsonde budget analysis during the TOGA COARE IOP. *J. Atmos. Sci.*, **53**, 1761-1780.

Frank, W. M., 1993: A hybrid parameterization with multiple closures. *The Representation of Cumulus Convection in Numerical Models.* K. Emanuel and D. Raymond, Eds, AMS, 151-154.

Fu, Q., S. K. Krueger, and K. N. Liou, 1995: Interactions of radiation and convection in simulated tropical cloud clusters. *J. Atmos. Sci.*, **52**, 1310-1328.

Gallus, W. A., Jr. and R. H. Johnson, 1991: Heat and moisture budgets of an intense midlatitude squall line. *J. Atmos. Sci.*, **48**, 122-146.

Gamache, J. F., and R. A. Houze, Jr., 1983: Water budget of a mesoscale convective system in the tropics. *J. Atmos. Sci.*, **40**, 1835-1850.

GEWEX Cloud System Study (GCSS), 1993: *Bull. Amer. Meteor. Soc.*, **74**, 387-400.

Grabowski, W. W., X. Wu, and M. W. Moncrieff, 1996: Cloud resolving modeling of tropical cloud systems during PHASE III of GATE. Part I: Two-dimensional experiments. *J. Atmos. Sci.*, **53**, 3684-3709.

Grabowski, W. W., X. Wu, M. W. Moncrieff, and W. D. Hall, 1998: Cloud resolving modeling of tropical cloud systems during PHASE III of GATE. Part II: Effects of resolution and the third dimension. *J. Atmos. Sci.*, **55**, 3264-3282.

Grabowski, W. W., X. Wu, and M. W. Moncrieff, 1999: Cloud resolving modeling of tropical cloud systems during PHASE III of GATE. Part III: Effects of cloud microphysics. *J. Atmos. Sci.*, **56**, 2384-2402.

Gray, W. M., and R. W. Jacobsen, 1977: Diurnal variation of deep cumulus convection. *Mon. Wea. Rev.*, **105**, 1171-1188.

Greco, S., J. Scala, J. Halverson, H. L. Massie, W.-K. Tao and M. Garstang, 1994: Amazon coastal squall lines. Part II: Heat and moisture transports. *Mon. Wea. Rev.*, **122**, 623-635.

Gregory, D., and M. J. Miller, 1989: A numerical study of the parameterization of deep tropical convection. *Quart. J. Roy. Mteor.*, **115**, 1209-1241.

Held, I. M., R. S. Hemler, and V. Ramaswamy, 1993: Radiative-convective equilibrium with explicit two-dimensional moist convection. *J. Atmos. Sci.*, **50**, 3909-3927.

Hill, G., 1974: Factors controlling the size and spacing of cumulus clouds as revealed by numerical experiments. *J. Atmos. Sci.*, **34**, 1934-1941.

Holle, R. L., and M. W. Maier, 1980: Tornado formation from downdraft interaction in the FACE mesonetwork. *Mon. Wea. Rev.*, **108**, 991-1009.

Houze, R. A., Jr., 1977: Structure and dynamics of a tropical squall-line system. *Mon. Wea. Rev.*, **105**, 1540-1567.

Houze, R. A., Jr., and C.-P. Cheng, 1977: Radar characteristics of tropical convection observed during GATE: mean properties and trends over the summer season. *Mon. Wea. Rev.*, **105**, 964-980.

Houze, R. A., Jr., 1982: Cloud clusters and large-scale vertical motions in the tropics. *J. Meteor. Soc. Japan*, **60**, 396-409.

Houze, R. A., Jr., and E. N. Rappaport, 1984: Air motions and precipitation structure of an early summer squall line over the eastern tropical Atlantic. *J. Atmos. Sci.*, **41**, 553-574.

Houze, R. A., Jr., 1989: Observed structure of mesoscale convective systems and implications for large-scale heating. *Quart. J. Roy. Meteor. Soc.*, **115**, 425-461.

Houze, R. A., Jr., 1997: Stratiform precipitation in regions of convection: A meteorological paradox. *Bull. Amer. Meteor. Soc.*, **78**, 2179-2196.

Johnson, D., W.-K. Tao, J. Simpson, and C.-H. Sui, 2000: A Study of the Response of Deep Tropical Clouds to Large-Scale Processes, Part I: Model Set-up Strategy and Comparison with observation, *J. Atmos. Sci.*, (submitted).

Johnson, R. H., 1984: Partitioning tropical heat and moisture budgets into cumulus and mesoscale components: Implication for cumulus parameterization. *Mon. Wea. Rev.*, **112**, 1656-1665.

Johnson, R. H., and P. J. Hamilton, 1988: The relationship of surface pressure features to the precipitation and airflow structure of an intense mid-latitude squall line.*Mon. Wea. Rev.*, **116**, 1444-1471.

Johnson, R. H., 1992: Heat and moisture sources and sinks of Asian Monsoon precipitating systems. *J. Meteor. Soc. Japan,* **70**, 353-371.

Johnson, R. H., and P. E. Ciesielski, 2000: Rainfall and radiative heating estimates from TOGA COARE atmospheric budgets. *J. Atmos. Sci.*, **57**, 1497-1514.

Khain, A. P., and I. Sednev, 1996: Simulation of precipitation formation in the Eastern Mediterranean coastal zone using a spectral microphysics cloud ensemble model. Atmospheric Research 43, 77-110.

Klemp, J. B., and R. Wilhelmson, 1978: The simulation of three-dimensional convective storm dynamics. *J. Atmos. Sci.*, **35**, 1070-1096.

Kogan, Y. L., and A. Shapiro, 1996: The simulation of a convective cloud in a 3D model with explicit microphysics. Part II: Dynamical and microphysical aspects of cloud merger. *J. Atmos. Sci.*, **53**, 2525-2545.

Kraus, E. B., 1963: The diurnal precipitation change over the sea. *J. Atmos. Sci.*, **20**, 546-551.

Krueger, S. K., 1988: Numerical simulation of tropical cumulus clouds and their interaction with the subcloud layer. *J. Atmos. Sci.*, **45**, 2221-2250.

Lafore, J.-P., and J.-L. Redelsperger, 1991: Effects of convection on mass and momentum fields as seen from cloud-scale simulations of precipitating systems. *ECMWF Workshop on Fine-scale Modelling and the Development of Parameterization Schemes,* September, Reading, U.K., 165-197.

Lafore, J.-P., J.-L. Redelsperger and G. Jaubert, 1988: Comparison between a three-dimensional simulation and Doppler radar data of a tropical squall line: Transport of mass, momentum, heat, and moisture. *J. Atmos. Sci.*, **45**, 3483-3500.

Lang, S., W.-K. Tao, J. Simpson and B. Ferrier, 2000: Numerical modeling of Convective-stratiform precipitation processes: Sensitivity to partition methods and numerical advection schemes, *Mon. Wea. Rev.*, (submitted).

Lau, K. M., C. H. Sui, and W.-K. Tao, 1993: A preliminary study of the tropical water cycle and its sensitivity to surface warming. *Bull. Amer. Meteor. Soc.*, **74**, 1313-1321.

Lau, K. M., C.-H. Sui, M.-D. Chou, and W.-K. Tao, 1994: An enquiry into the cirrus-cloud thermostat effect for tropical sea surface temperature. *Geophys. Res. Lett.*, **21**, 1157-1160.

Leary, C. A., and R. A. Houze, Jr., 1980: The contribution of mesocale motions to the mass and heat fluxes of an intense tropical convective system. *J. Atmos. Sci.*, **37**, 784-796.

LeMone, M. A. and E. J. Zipser, 1980: Cumulonimbus vertical velocity events in GATE. Part I: Diameter, intensity and mass flux. *J. Atmos. Sci.*, **37**, 2444-2457.

LeMone, M. A., 1989: The influence of vertical wind shear on the diameter of cumulus clouds in CCOPE. *Mon. Wea. Rev.*, **117**, 1480-1491.

LeMone, M. A., G. M. Barnes, J. C. Fankhauser and L. F. Tarleton, 1988: Perturbation pressure fields measured by aircraft around the cloud-base updraft of deep convective clouds. *Mon. Wea. Rev.*, **116**, 313-327.

Li, X., C.-H. Sui, K.-M. Lau and M.-D. Chou, 1999: Large-scale forcing and cloud-radiation interaction in the tropical deep convective regime. *J. Atmos. Sci.*, **56**, 3028-3042.

Lin, X., and R. H. Johnson, 1996: Heating, moistening and rainfall over the western Pacific during TOGA COARE. *J. Atmos. Sci.*, **53**, 3367-3383.

Lin, Y.-L., R. D. Farley, and H. D. Orville, 1983: Bulk parameterization of the snow field in a cloud model. *J. Clim.ate Appl. Meteor.*, **22**, 1065-1092.

Lipps, F. B., and R. S. Helmer, 1986: Numerical simulation of deep tropical convection associated with large-scale convergence. *J. Atmos. Sci.*, **43**, 1796-1816.

List, R., and R. S. Schemenauer, 1971: Free-fall behavior of planar snow crystals, conical graupel and small hail. *J. Atmos. Sci.*, **28**, 110-115.

Liu, C., and M. W. Moncrieff, 1998: A numerical study of the diurnal cycle of tropical oceanic convection. *J. Atmos. Sci.* **55**, 2329-2344.

Lopez, R. E., 1978: Internal structure and development processes of c-scale aggregates of cumulus clouds. *Mon. Wea. Rev.*, **106**, 1488-1494.

Lynn, B. H., W.-K. Tao and P. Wetzel, 1998: A study of landscape generated deep moist convection, *Mon. Wea. Rev.* , **126**, 928-942.

Lynn, B. H., W.-K. Tao and F. Abramopoulos, 2000a: A parameterization for the triggering of landscape generated moist convection, Part I: Analyses of high resolution model results, *J. Atmos. Sci.*, (in press).

Lynn, B. H., and W.-K. Tao, 2000b: A parameterization for the triggering of landscape generated moist convection, Part II: Zero order and first order closure, *J. Atmos. Sci.*, (in press).

Malkus, J. S., 1954: Some results of a trade cumulus clouds investigation. *J. Meteor.*, **11**, 220-237.

Malkus, J. S. and H. Riehl, 1964: *Cloud Structure and Distributions Over the Tropical Pacific Ocean.* University of California Press, 229 pp.

McCumber, M., W.-K. Tao, J. Simpson, R. Penc, and S.-T. Soong, 1991: Comparison of ice-phase microphysical parameterization schemes using numerical simulations of convection. *J. Appl. Meteor.*, **30**, 985-1004.

Miller, R. A., and W. M. Frank, 1993: Radiative forcing of simulated tropical cloud clusters. *Mon. Wea. Rev.*, **121**, 482-498.

Miller, M. J., and R. P. Pearce, 1974: A three-dimensional primitive equation model of cumulonimbus and squall lines. *Quart. J. R. Met. Soc.*, **100**, 133-154.

Molinari, J., and M. Dudek, 1992: Parameterization of convective precipitation in mesoscale numerical models: A critical review. *Mon. Wea. Rev.*, **120**, 326-344.

Moncrieff, M. W., 1992: Organized convective systems: Archetypal dynamical models, momentum flux theory, and parameterization. *Quart. J. Roy. Meteor. Soc.*, **118**, 819-850.

Moncrieff, M. W., S. K. Krueger, D. Gregory, J.-L. Redelsperger and W.-K. Tao, 1997: GEWEX Cloud System Study (GCSS) Working Group 4: Precipitating convective cloud systems, *Bull. Amer. Meteor. Soc.*, **78**, 831-845.

Moncrieff, M. W., and W.-K. Tao, 1999: Cloud-resolving models, *Global Water and Energy Cycles*, Ed. by K. Browing and R. J. Gurney, *Cambridge University Press*, 200-209.

Nakazawa, T., 1988: Tropical super clusters within intraseasonal variations over the western Pacific. *J. Meteor. Soc.*, Japan, **66**, 823-839.

Nikajima, K., and T. Matsuno, 1988: Numerical experiments concerning the origin of cloud cluster in tropical atmosphere. *J. Meteor. Soc. Japan*, **66**, 309-329.

Newton, C. W., 1966: Circulations in large sheared cumulonimbus. *Tellus*, **18**, 699-712.

Ogura, Y., and J. G. Charney, 1962: A numerical model of thermal convection in the atmosphere. *Met. Soc. of Japan*, **40,** 431-451.

Ogura, Y., and N. A. Phillips, 1962: Scale analysis of deep and shallow convection in the atmsphere. *J. Atmos. Sci.*, **19**, 173-179.

Ogrua, Y., and J.-Y. Jiang, 1985: A modeling study of heating and drying effects of convective clouds in an extratropical mesoscale system. *J. Atmos. Sci.*, 42, 2478-2492.

Orville, H. D., Y.-H. Kuo, R. D. Farley and C. S. Hwang, 1980: Numerical simulation of cloud interactions. *J. Rech. Atmos.*, **14**, 499-516.

Pickering, K. E., J. R. Scala, A. M. Thompson, W.-K. Tao, and J. Simpson, 1992: A regional estimate of convective transport of CO from biomass burning. *Geophys. Res. Lett.*, **19**, 289-292.

Prasad, N, H.-Y. M. Yeh, R. F. Adler and W.-K. Tao, 1995: Infrared and microwave simulations of an intense convective system and comparison with aircraft observations. *J. Appl. Meteor.*, **34**, 153-174.

Randall, D. A., Harshvardhan, and D. A., Dazlich, 1991: Diurnal variability of the hydrologic cycle in a general circulation model. *J. Atmos. Sci.*, **48**, 40-62.

Riehl, H. and J. S. Malkus, 1958: On the heat balance in the equatorial trough zone. *Geophysica*, **6**, 503-535.

Riehl, H. and J. Simpson, 1979: The heat balance of the equatorial trough zone, revisited. *Beitr. Phys. Atmos.*, **52**, 287-305.

Rotunno, R., J. B. Klemp and M. L. Weisman, 1988: A theory for strong, long-lived squall lines. *J. Atmos. Sci.*, **45**, 463-485.

Rutledge, S.A., and P.V. Hobbs, 1984: The mesoscale and microscale structure and organization of clouds and precipitation in mid-latitude clouds. Part XII: A diagnostic modeling study of precipitation development in narrow cold frontal rainbands. *J. Atmos. Sci.*, **41**, 2949-2972.

Rutledge, S. A., 1986: A diagnostic modeling study of the stratiform region associated with a tropical squall line. *J. Atmos. Sci.*, **43**, 1356-1377.

Rutledge, S. A., and R. A. Houze, Jr., 1987: A diagnostic modeling study of the trailing stratiform rain of a mid latitude squall line. *J. Atmos. Sci.*, **44**, 2640-2656.

Scala, J. R., M. Garstang, W.-K. Tao, K. E. Pickering, A. M. Thompson, J. Simpson, V. W. J. H. Kirchoff, E. V. Browell, G. W. Saschse, A. L. Torres, G. L. Gregory, R. A. Rasmussen, and M. A. K. Khalil, 1990: Cloud draft structure and trace gas transport. *J Geophys. Res.*, **95**, 17015-17030.

Schlesinger, R. E., 1975: A three-dimensional numerical model of an isolated deep convective cloud. Preliminary results. *J. Atmos. Sci.*, **32**, 934-957.

Schlesinger, R. E., 1978: A three-dimensional numerical model of an isolated thunderstorm: Part I. Comparative experiments for variable ambient wind shear. *J. Atmos. Sci.*, **35**, 690-713.

Scorer, R. S., and F. H. Ludlam, 1953: Bubble theory of penetrative convection. *Quart. J. Roy. Meteor. Soc.*, **79**, 94-103.

Shie, C.-L., W.-K. Tao, J. Simpson, D. Johnson and C.-H. Sui, 2000: A sensitivity study of equilibrium states simulated by a cloud-resolving model, *J. of Climate,* (submitted).

Short, D. A., B. S. Ferrier, J. C. Gerlach, S. A. Rutledge, and O. W. Thiele, 1997: Shipboard radar rainfall patterns within the TOGA COARE IFA. *Bull. Amer. Meteor. Soc.*, **78**, 2817 - 2836.

Simpson, J., 1980: Downdrafts as linkages in dynamic cumulus seeding effects. *J. Appl. Meteor.*, **19**, 477-487.

Simpson, J., N. E. Westcott, R. J. Clerman, and R. A. Pielke, 1980: On cumulus mergers. *Arch. Meteor. Geophys. Bioklimator*, **A29**, 1-40.

Simpson, J., R. F. Adler, and G. R. North, 1988: A proposed tropical rainfall measuring mission (TRMM) satellite. *Bull. Amer. Meteor. Soc.*, **69**, 278-295.

Simpson, J., and W.-K. Tao, 1993: The Goddard Cumulus Ensemble Model. Part II: Applications for studying cloud precipitating processes and for NASA TRMM. *Terrestrial, Atmospheric and Oceanic Sciences*, **4**, 73-116.

Simpson, J., T. D. Keenan, B. Ferrier, R. H. Simpson, and G. J. Holland, 1993: Cumulus mergers in the Maritime continent region, *Meteor. and Atmos. Phys.* , **51**, 73-99, 1993.

Simpson, J., C. Kummerow, W.-K. Tao, and R. Adler, 1996: On the Tropical Rainfall Measuring Mission (TRMM), *Meteor. and Atmos. Phys.* , **60**, 19-36, 1996.

Smolarkiewicz, P. K., and W. W. Grabowski, 1990: The multidimensional positive advection transport algorithm: Nonoscillatory option. *J. Comput. Phys.*, **86**, 355-375.

Smull, B. F., and R. A. Houze, Jr., 1987: Rear inflow in squall lines with trailing stratiform precipitation. *Mon. Wea. Rev.*, **115**, 2869-2889.

Sommeria, G., 1976: Three-dimensional simulation of turbulent processes in an undisturbed trade wind boundary layer. *J. Atmos. Sci.*, **33**, 216-241.

Soong, S.-T., and Y. Ogura, 1980: Response of trade wind cumuli to large-scale processes. *J. Atmos. Sci.* , **37**, 2035-2050.

Soong, S.-T., and W.-K. Tao, 1980: Response of deep tropical clouds to mesoscale processes. *J. Atmos. Sci.* , **37** 2016-2036.

Soong, S.-T., and W.-K. Tao, 1984: A numerical study of the vertical transport of momentum in a tropical rainband. *J. Atmos. Sci.*, **41**,1049-1061.

Stephens, G. L., 1983: The influence of radiative transfer on the mass and heat budget of ice crystals falling in the atmosphere. *J. Atmos. Sci.*, **40**, 1729-1739.

Sui, C.-H., and K.-M. Lau, 1989: Origin of low-frequency (Intraseasonal) oscillations in the tropical atmosphere. Part II: Structure and propagation of mobile wave-CISK modes and their modification by lower boundary forcings. *J. Atmos. Sci.*, **46**, 37-56.

Sui, C. H., K. M. Lau, W.-K. Tao, and J. Simpson, 1994: The tropical water and energy cycles in a cumulus ensemble model. Part I: Equilibrium climate. *J. Atmos. Sci.*, **51**, 711-728.

Sui, C. H., K. M. Lau, and X. Li, 1998: Convective-radiative interaction in simulated diurnal variations of tropical cumulus ensemble. *J. Atmos. Sci.*, **55**, 2345-2357.

Tao, W.-K., 1978: A numerical simulation of deep convection in the tropics, M.S. Thesis, Department of Atmospheric Science, University of Illinois, 66 pp..

Tao, W.-K., 1983: A numerical study of the structure and vertical transport properties of a tropical convective system. Ph.D. Dissertation, Department of Atmospheric Science, University of Illinois, 228 pp.

Tao, W.-K., and J. Simpson, 1984: Cloud interactions and merging: Numerical simulations. *J. Atmos. Sci.,* **41**, 2901-2917.

Tao, W.-K., and S.-T. Soong, 1986: A study of the response of deep tropical clouds to mesoscale processes: Three-dimensional numerical experiments. *J. Atmos. Sci.*, **43**, 2653-2676.

Tao, W.-K., J. Simpson, and S.-T. Soong, 1987: Statistical properties of a cloud ensemble: A numerical study. *J. Atmos. Sci.*, **44**, 3175-3187.

Tao, W.-K., and J. Simpson, 1989a: A further study of cumulus interaction and mergers: Three-dimensional simulations with trajectory analyses. *J. Atmos. Sci.*, **46**, 2974-3004.

Tao, W.-K., and J. Simpson, 1989b: Modeling study of a tropical squall-type convective line. *J. Atmos. Sci.*, **46**, 177-202.

Tao, W.-K., J. Simpson and M. McCumber, 1989: An ice-water saturation adjustment. *Mon. Wea. Rev.*, **117**, 231-235.

Tao, W.-K., J. Simpson, S. Lang, M. McCumber, R. Adler and R. Penc, 1990: An algorithm to estimate the heating budget from vertical hydrometeor profiles. *J. Appl. Meteor.*, **29**, 1232-1244.

Tao, W.-K., J. Simpson, and S.-T. Soong, 1991: Numerical simulation of a sub-tropical squall line over Taiwan Strait. *Mon. Wea. Rev.*, **119**, 2699-2723.

Tao, W.-K., J. Simpson, C.-H. Sui, B. Ferrier, S. Lang, J. Scala, M.-D. Chou, and K. Pickering, 1993a: Heating, moisture and water budgets of tropical and mid-latitude squall lines: Comparisons and sensitivity to longwave radiation. *J. Atmos. Sci.*, **50**, 673-690.

Tao, W.-K., J. Simpson, S. Lang, J. Simpson and R. Adler, 1993b: Retrieval Algorithms for estimating the vertical profiles of latent heat release: Their applications for TRMM. *J. Meteor. Soc. Japan* , **71**, 685-700.

Tao, W.-K., and J. Simpson, 1993: The Goddard Cumulus Ensemble Model. Part I: Model description. *Terrestrial, Atmospheric and Oceanic Sciences*, **4**, 19-54.

Tao, W.-K., J. Scala, B. Ferrier ,and J. Simpson, 1995: The effects of melting processes on the development of a tropical and a mid-latitudes squall line. *J. Atmos. Sci.*, **52**, 1934-1948.

Tao, W.-K., 1995: Interaction of parameterized convection and explicit stratiform cloud microphysics. WMO/WCRP-90, Cloud Microphysics Parameterizations in Global Atmospheric General Circulation Models, Ed. D. Randall, 199-210.

Tao, W.-K., S. Lang, J. Simpson, C.-H. Sui and B. Ferrier and M.-D. Chou, 1996: Mechanisms of Cloud-radiation interaction in the tropics and midlatitudes. *J. Atmos. Sci.* **53**, 2624-2651.

Tao, W.-K., J. Simpson and B. Ferrier, 1997: Cloud Resolving Model Simulations of Mesoscale Convective Systems, *New Insights and Approaches to Convective Parameterization*, Ed. D. Gregory, 77-112.

Tao, W.-K., J. Simpson, C.-H. Sui, C.-L. Shie, B. Zhou, K. M. Lau, and, M. Moncrieff, 1999: On equilibrium states simulated by Cloud-Resolving Models, *J. Atmos. Sci.*, **56**, 3128-3139.

Tao, W.-K., S. Lang, J. Simpson, W. S. Olson, D. Johnson, B. Ferrier, C. Kummerow and R. Adler, 2000a: Vertical profiles of latent heat release and their retrieval in TOGA COARE convective systems using a cloud resolving model, SSM/I and radar data, *J. Meteor. Soc. Japan,* (August Issue).

Tao, W.-K., S. Lang, W. S. Olson, S. Yang, R. Meneghini, J. Simpson, E. Smith, C. Kummerow, E. Smith and J. Halverson, 2000b: Retrieved Vertical Profiles of Latent Heat Release Using TRMM Products for February 1998, *J. Appl. Meteor.* (conditionally accepted).

Tao, W.-K., C.-L. Shie and J. Simpson, 2000c: Comments on The sensitivity study of radiative-convective equilibrium in the Tropics with a convective resolving model, *J. Atmos. Sci.* (accepted).

Thompson, A. M., W.-K. Tao, K. E. Pickering, J. Scala, and J. Simpson, 1997: Tropical deep convection and ozone formation, *Bull. Amer. Meteor. Soc.*, **78**, 1043-1054.

Thompson, R. M., Jr., S. W. Payne, E. E. Recker, and R. J. Reed, 1979: Structure and properties of synoptic-scale wave disturbances in the intertropical convergence zone of the eastern Atlantic. *J. Atmos. Sci.*, **36**, 53-72.

Turpeinen, O., 1982: Cloud interactions and merging on day 261 of GATE. *Mon. Wea. Rev.*, **110**, 1238-1254.

Wang, Y., W.-K. Tao, and J. Simpson, 1996: The Impact of a surface layer on a TOGA COARE cloud system development. *Mon. Wea. Rev.* **124**, 2753-2763.

Wang, Y., W.-K. Tao, J. Simpson, and S. Lang, 2000: The sensitivity of tropical squall lines (GATE and TOGA COARE) to surface fluxes: Cloud resolving model simulations, *Q. J. R. Met. Soc.* (submitted).

Webster, P. J., and G. L. Stephens, 1980: Tropical upper troposphere extended clouds: Inferences from Winter MONEX. *J. Atmos. Sci.*, **37**, 1521-1541.

Westcott, N., 1984: A historical perspective on cloud mergers. *Bull. Amer. Meteor. Soc.*, **65**, 219-226.

Wilhelmson, R., 1974: The life cycle of a thunderstorm in three dimensions. *J. Atmos. Sci.*, 31, 735-743.

Wilkins, E. M., Y. K. Sasaki, G. E. Gerber and W. H. Chaplin, Jr., 1976: Numerical simulation of the lateral interactions between buoyant clouds. *J. Atmos. Sci.*, **33**, 1321-1329.

Wong, T., G. L. Stephens, P. W. Stackhouse, Jr., and F. P. J. Valero, 1993: The radiative budgets of a tropical mesoscale convective system during the EMEX-STEP Experiment. 2. Model results. *J. Geophy. Res.*, **98**, 8695-8711.

Wu, X., and M. W. Moncrieff, 1996: Recent progress on cloud-resolving modeling of TOGA COARE and GATE cloud systems. *New Insights and Approaches to Convective Parameterization,* ECMWF, Reading, United Kingdom, 128-156.

Wu, X., W. W. Grabowski and M. W. Moncrieff, 1998: Long-term behavior of cloud systems in TOGA COARE and their interactions with radiative and surface processes. Part I: Two-dimensional modeling study. *J. Atmos. Sci.*, **55**, 2693-2714.

Wu, X., W. W. D. Hall, W. Grabowski and M. W. Moncrieff, 1999: Long-term behavior of cloud systems in TOGA COARE and their interactions with radiative and surface processes. Part II: Effects of ice microphysics on cloud-radiation interaction. *J. Atmos. Sci.*, **56**, 3177-3195

Xu, K.-M., and D. A. Randall, 1995: Impact of interactive radiative transfer on the microscopic behavior of cumulus ensembles. Part II: Mechanisms for cloud-radiation interactions. *J. Atmos. Sci.*, **52**, 800-817.

Xu, K.-M., and D. A. Randall, 1996: Explicit simulation of cumulus ensembles with the GATE Phase III data: Comparison with observations. *J. Atmos. Sci.*, 53, 3709-3736.

Yanai, M., S. Esbensen, and J. Chu, 1973: Determination of average bulk properties of tropical cloud clusters from large-scale heat and moisture budgets *J. Atmos. Sci.*, **30**, 611-627.

Yau, M. K., and R. Michaud, 1982: Numerical simulation of a cumulus ensemble in three dimensions. *J. Atmos. Sci.*, **39**, 1062-1079.

Yeh, H.-Y., M. N. Prasad, R. Meneghini, W.-K. Tao and R.F. Adler, 1995: Model-based simulation of TRMM spaceborne radar observations. *J. Appl Meteor.*, **34**, 175-197.

Zipser, E. J., 1969: The role of organized unsaturated convective downdrafts in the structure and rapid decay of an equatorial disturbance. *J. Appl. Meteor.*, **8**, 799-814.

Zipser, E. J., 1977: Mesoscale and convective-scale downdrafts as distinct components of squall-line structure. *Mon. Wea. Rev.*, **105**, 1568-1589.

Zipser, E. J. and M. A. LeMone, 1980: Cumulonimbus vertical velocity events in GATE. Part II: Synthesis and model core structure. *J. Atmos. Sci.*, **37**, 2458-2469.

Zipser, E. J., R. J. Meitin and M. A. LeMone, 1981: Mesoscale motion fields associated with a slowly moving GATE convective band. *J. Atmos. Sci.*, **38**, 1725-1750.

Table Captions

Table 1 Major foci of cloud resolving model (CRM) development in the past four decades. Some (by no means all) key contributors are also listed. (The author apologizes for omitting any other major contributors to CRM development.)

Table 2 Key developments in the cloud resolving model (CRM) approach for studying tropical deep convective systems over the past two decades.

Table 3 Characteristics of the Goddard Cumulus Ensemble Model

Table 4 Applications of the Goddard Cumulus Ensemble (GCE) Model. The specific topics and their respective GCE model characteristics, major results and references are shown.

Table 5 Initial environmental conditions expressed in terms of CAPE, precipitable water and Richardson number for the TAMEX, EMEX, TOGA COARE and PRE-STORM MCSs.

Table 6 Values of the ratio R for the GCE model simulations of several convective systems, as well as for the 6 h periods corresponding to the initial and mature stages. Their respective stratiform rain components are shown in the first column.

Table 7 The same ratio defined in Table 3.2.2 except for different MCS cases, A, B and C of Leary and Houze (1980), cases I and II of Gamache and Houze (1983), the 10-11 June squall line of Gallus and Johnson (1991), and the COPT squall line of Chong and Hauser (1989). Ratios from other CRM studies of convective-stratiform interaction are also shown.

Table 8 Summary of previous cloud-radiation modeling study results. The percentage increase or decrease in surface precipitation due to longwave and shortwave effects are given along with the mesoscale lifting, if used, for each case.

Table 9 Ratio of fractional cloud coverage (R = cloud updraft coverage / cloud downdraft coverage). Fractional coverage occupied by cloud drafts and active cloud drafts over the domain are also shown within the parentheses. This figure is from Tao, Simpson and Tao (1987).

Table 10 The GCE model simulated domain averaged surface rainfall (mm), stratiform amount (percentage) and microphysical processes (ratios between evaporation and condensation, sublimation and deposition, and deposition and condensation). (a) is for TOGA COARE and (b) for GATE. For TOGA COARE, the GCE model results are also separated into sub-periods, deep strong convection during December 20-23 and 24-25 and weaker convection prior to, in between, and after the deep convection (December 19-20, 23-24, and 25-26, 1992). Slow-moving (non-squall, September 2-4), fast-moving (squall, September 4 to 6) and less organized (September 6 to 8) periods for the GCE model simulated GATE results are also shown.

Figure Captions

Fig. 1 Estimated surface rainfall intensity over part of horizontal domain at **(a)** 270 min, **(b)** 285 min, **(c)** 300 in and **(d)** 315 min simulated time from a three-dimensional GCE model. The contour interval is 10 mm h^{-1} starting at 1 mm h^{-1}. This type of merger is identified as a parallel cells case.

Fig. 2 Same as Fig. 3.1.1 except for the case of perpendicular cells. Time is **(a)** 255 min, **(b)** 270 min, **(c)** 285 min and **(d)** 300 min.

Fig. 3 Depiction of trajectory paths calculated from the evolving three-dimensional model wind fields for the parallel cell case shown in Fig. 3.1.1. **(a)** Three-dimensional depiction of upward paths as viewed from NNW, **(b)** as viewed from the overhead. They are computed forward from 300 min to 340 min. **(c)** and **(d)** are the same as (a) and (b). respectively, except they are computed backward from 300 min to 270 min. The shaded area in (a) and (c) indicates the three-dimensional depiction of estimated 20 dBZ iso-surface at 300 min.

Fig. 4 **(a)** and **(b)** are schematic cross-sections through mature squall lines observed in the tropics and midlatitudes, respectively. They are adopted from Houze (1977) and Smull and Houze (1987). **(c)** and **(d)** are the schematic diagrams of major conceptual models of tropical and midlatitude squall lines derived from case studies, respectively. Areas of light and dark stippling indicate areas of high- and low-θ_e air, respectively. They are originally shown in Zipser (1969) and Newton (1963), but are adopted from Rotunno *et al.* (1988).

Fig. 5 The water budgets for **(a)** TAMEX, **(b)** EMEX, **(c)** PRE-STORM and **(d)** TOGA COARE simulated squall-line MCSs. Italic numbers indicate the amount of condensate transfer between various regions and layers while quantities in parenthese are the net condensation generated through microphysical processes.

Fig. 6 Schematic diagram demonstrating the effects by different cloud-radiation mechanisms (cloud-top cooling and cloud-base warming - alters the thermal stratification of the stratiform cloud layer; differential cooling between clear and cloudy regions - enhances dynamic convergence into the cloud system; and the large-scale radiative cooling - destabilizes the large-scale environment).

Fig. 7 **(a)** Convective and **(b)** stratiform heating profiles stored in the heating profile look-up table for the CSH algorithm. The profiles were obtained from GCE model simulations for cloud systems in various geographic locations [the Pacific warm pool region (TOGA1, TOGA2, TOGA3, ERECT - a squall system with erect updrafts, MRSH ISL - Marshall Island), the East Atlantic region (GATE), midlatitude USA (PRESTORM - PSTM), and Australia (EMEX)]. **(c)** and **(d)** are the same as **(a)** and **(b)** except that these profiles are from Gallus and Johnson (1991, curve GJ), Yanai et al. (1973) but partitioned into convective and stratiform components by Johnson (1984, curve Y), Houze (1989, curve H), Houze and Rappaport (1984, curve HR), Chong and Hauser (1990, curve CH) and an African squall line simulated by Caniaux et al. (1994, curve COPT81).

Fig. 8 Monthly (February 1998) mean latent heating at **(a)** 8, **(b)** 5 and **(c)** 2 km over the global tropics derived from the CSH algorithm.

Fig. 9 Heating rates for condensation, **c**, and evaporation, **e**, in the two-dimensional model (dashed line) and the three-dimensional model (solid line). The heating rate estimated from the large-scale observations, Q_1 - Q_R, and the total cloud heating rate in the three-dimensional model are also included. This figure is from Tao, Simpson and Tao (1987).

Fig. 10 **(a)** The vertical profiles of the heating rate by condensation of moisture, c, evaporation of liquid water drops, e, net vertical flux of the sensible heat, F, the total heating rate by clouds and the heating rate estimated from large-scale observations, Q_1 - Q_R. **(b)** The vertical profiles of the moistening rate by condensation of moisture, evaporation from liquid water drops, net vertical moisture flux, the total moistening rate by clouds and the moistening rate estimated from the large-scale observations, - $(c_p/L)Q_2$. This result was from a 3-D GCE model simulation for a GATE convective system (Tao and Soong, 1986).

Fig. 11 Time sequence of the GCE model estimated domain mean surface rainfall rate (mm h^{-1}) for (a) TOGA COARE and (b) GATE. This type of CRM diagnostics and graphical presentation have been very popular were first presented in Tao and Simpson (1984).

	Major foci	Key Contributors
1960's	Loading, Buoyancy and Entrainment	J. Simpson (1st 1D model) Y. Ogura and N. Pillips (1st 2D anelastic)
1970's	Slab- vs axis-symmetric model 2D vs 3D Cloud Seeding Super Cell Dynamics Cloud Dynamics & Warm rain	T. Clark, W. Cotton, E. Kessler, J. Klemp, M. Miller, M. Moncrieff, H. D. Orville, R. Schlesinger, G. Sommeria, S.-T. Soong, R. Wilhelmson and others
1980's	Ensemble of clouds - cumulus parameterization Cloud interactions and mergers Ice processes Convective and stratiform Cloud Dynamics - Wind Shear Large-scale and cloud-scale interactions Cloud Radiation Interaction	N. A. Crook, K. K. Droegemeier, J. Dudhia, D. Durran, R. D. Farley, R. Fovell, B. Ferrier, S. Krueger, Y.-L. Lin, R. Rotunno, W. Skamarock, W.-K. Tao, G. J. Tripoli, M. L. Weisman and many others
1990's	Land and ocean processes Multi-scale interactions Cloud Chemistry Process modeling - Climate Variation Implications GEWEX Cloud System Study (GCSS) Coupled with microwave radiative model for TRMM	Many young and talented scientists

Table 1

Tao, Simpson & Soong (1987)	2-D 3-D	Water	TKE K-theory	128 km 32 x 32 km^2	16 h 6 h
Nikajima & Matsuno (1988)	2-D 3-D	Water	TKE	32-64 km 24 x 16 km^2	4 h
Dudhia & Moncrieff (1987)	2-D 3-D	Water		128 km 32 x 32 km^2	6 h
Krueger (1988)	2-D	Water	K-theory Prescribed fluxes	512 km	6 h
Tao & Simpson (1989)	2-D 3-D	Water Water & Ice	3rd Moment	25 x 50 km^2 30 km	50 h 3 h
Gregory & Miller (1989)	2-D		TKE	512 km	2 h
Xu & Krueger (1991)	2-D	Water	Prescribed fluxes	96 x 96 km^2	12 h
McCumber, Tao, Simpson, Penc & Soong (1992)	2-D 3-D	Water & Ice	3rd moment	256 km 512 km	4 h 9 h
Xu, Arakawa & Krueger (1992), Xu and Arakawa (1992), Xu (1994)	2-D	Water Water & Ice	TKE	512 km	120 h
Held, Hemler & Ramaswamy (1993)	2-D	Water & Ice	3rd moment	64 x 32 km^2	12 h 3 h
Sui, Lau, Tao, Simpson & Chou (1994)	2-D	Water & Ice	K-theory	512 km	120 h
Grabowski, Wu & Moncrieff (1996, 1999) and Grabowski, Wu Moncrieff & Hall (1998)	2-D 3-D	Water & Ice	TKE	640 km	1000 h
Xu (1995), Xu and Randall (1996a,b)	2-D	Water & Ice	K-theory	768 km	1248 h
Donner, Seman & Hemler (1999)	3-D	Water & Ice	3rd Moment	900 km 400 x 400 km^2	7 days
Xu, Grabowski & Moncrieff (1998)	2-D	Water & Ice	K-theory	512 km	18 days
Li, Sui, Lau & Chou (1999)	2-D	Water & Ice	K-theory	220 x 200 km^2	73 h
Su, Chen & Bretherton (1999)	3-D	Water & Ice	TKE	900 km	39 days
Johnson, Tao, Simpson & Sui (2000)	2-D	Water & Ice	Blackadar-Type TKE	768 km 210 x 210 km^2 1024 km	7 days 7 days 7 days

Table 2

Parameters/Processes	GCE Model
Vertical Coordinate	z
Explicit Convective Processes	2 class water & 2 moment 4 class ice
Implicit Convective Processes	Betts and Miller, Kain and Frisch
Numerical Methods	Positive Definite Advection for Scalar Variables; 4-th Order for Dynamic Variables
Initialization	Initial Condition with Forcing from Observations/Large-Scale Model
Radiation	Broad-Band in LW; Solar Explicit Cloud-radiation Interaction
Sub-Grid Diffusion	TKE
Two-Way Interactive Nesting	Radiative-Type (2D model only)
Surface Energy Budget	Force-restore Method 7-Layer Soil Model (PLACE) TOGA COARE Flux Module

Table 3

Topics	**Model Characteristics**	**Major Results**	**References**
Cloud-Cloud Interactions and Mergers	2D/3D Warm rain	Cloud downdraft and its associated cold outflow play major role in cloud merger	Tao and Simpson (1984, 1989a)
Q_1 and Q_2 Budgets	2D/3D Warm rain and Ice Processes	Importance of evaporative cooling in Q_1 budget Importance of vertical transport of moisture by convection in Q_2 budget	Tao (1978), Soong and Tao (1980), Soong and Tao (1986), Tao and Simpson (1989b), Tao *et al.* (1991, 1993a, 1996), Johnson *et al* (2000)
Cloud Characteristics	2D/3D Warm rain	Active convective updrafts cover small area but major contributors in mass, Q_1 and Q_2 budgets. Excellent agreement with aircraft measurements.	Tao and Soong (1986), Tao *et al.* (1987)
Convective Momentum Transport	2D/3D Smaller Domain in 3D	Identify the role of horizontal pressure gradient force on up-gradient transport of momentum.	Soong and Tao (1984), Tao and Soong (1986), Tao *et al.* (1995)
Ice Processes	2D/3D	The importance of ice processes for stratiform rain formation and its associated mass, Q_1 and Q_2 budgets.	Tao and Simpson (1989), McCumber *et al.* (1991), Tao *et al.* (1993a), Ferrier *et al.* (1995)
Convective and Stratiform Interactions	2D	The horizontal transport of hydrometeors and water vapor from convective towers to stratiform region are quantified.	Tao *et al.* (1993a), Sui *et al.* (1994), Tao (1995), Lang *et al.* (2000)
Cloud Radiation Interactions & diurnal variation of precipitation	2D (short and long term integration)	Longwave cooling can enhance precipitation significantly for tropical cloud systems, but only slightly for midlatitude systems. Modulation in relative humidity by radiative processes is major reason for diurnal variation of precipitation.	Tao *et al.* (1993a), Tao *et al.* (1996), Sui *et al.* (1998)
Cloud Chemistry Interactions	2D/3D	Significant redistribution of trace gases by convection. Enhancement of O_3 production related to deep convection in tropics.	Thompson *et al* (1997 - a review)
Air-Sea Interactions	2D/3D	TOGA COARE flux algorithm performs well compared with observation, better than other flux algorithms. Surface fluxes are important for precipitation processes and maintain CAPE and boundary layer structure.	Wang *et al.* (1996, 2000)
Precipitation Efficiency (PE)	2D	Examined different definitions of PE. Identify several important atmospheric parameters for better PE.	Ferrier *et al.* (1996)

Table 4

Land Processes	2D/3D	Importance of mesoscale circulation induced by soil gradient on precipitation. Identify the atmospheric parameters for triggering convection.	Lynn *et al.* (1998, 2000a, b), Baker *et al.* (2000)
Idealized Climate Variations in Tropics	2D	Examined several important hypotheses associated with climate variation and climate warming. Identified physical processes that cause two different statistical equilibrium states (warm/humid and cold/dry) in idealized climates.	Sui e*t al* (1994), Lau *et al* (1994, 1995) Tao *et al.* (1999, 2000), Shie *et al.* (2000)
TRMM Rainfall Retrieval	3D	Improved the performance of TRMM rainfall retrieval algorithms by providing realistic cloud profiles.	Simpson *et al.* (1996 - a review)
Latent Heating Profile Retrieval	2D	Developed algorithms for retrieving four dimensional vertical structure of latent heating profiles over global tropics,	Tao *et al.* (1990, 1993b, 2000a, b)

Table 4 (Cont.)

	CAPE m^2s^{-2}	PrecipitableWater ($g\ cm^{-2}$)	Richardson Number	$\Delta x, \Delta z$ (m) (L_x, L_z) (km)	References
TAMEX	1450	5.275	29	750, 240-1150 (1906, 22)	Tao *et al* 1991
EMEX	1484	6.175	555	750, 240-1150 (1906, 22)	Tao *et al* 1993
PRESTORM	2300	4.385	43	1000, 225-1000 (2542, 20)	Tao *et al* 1993
TOGA COARE	1776	6.334	74	750, 40-1100 (1906, 22)	Wang *et al* 1996

Table 5

$$Ratio = \frac{C_T}{C_T + C_M}$$

	Stratiform (0-12 h)	Ratio (0-12 h)	Initial -Stage (0-6 h)	Mature- Stage (6-12 h)
COARE	42.3%	0.40	0.46	0.36
EMEX	49.1%	0.41	0.47	0.35
TAMEX	29.6%	0.37	0.43	0.33
PRESTORM	22.5%	0.54	0.82	0.43

Table 6

$$Ratio = \frac{C_T}{C_T + C_M}$$

	Ratio	Stratiform Amount (%)	Case
Leary and Houze (1980)	**1.00**	**40%**	Tropics (GATE)
Leary and Houze (1980)	**1.00**	**40%**	Tropics (GATE)
Leary and Houze (1980)	**0.50**	**40%**	Tropics (GATE)
Gamache and Houze (1983)	**0.55**	**49%**	Tropics (GATE)
Gamache and Houze (1983)	**0.64**	**49%**	Tropics (GATE)
Gallus and Johnson (1991)	**0.37**	**30%**	Midlatitude (PRESTORM)
Chong and Hauser (1989)	**0.47**	**40%**	COPT 81 June 22
Chin (1994)	***0.90***	*10%*	Midlatitude
Chin *et al* (1995)	***0.37***	*39%*	Tropics (GATE)
Caniaux *et al* (1994)	***0.22 (4-5 h)*** ***0.09 (7-8 h)***	*17%* *44%*	COPT 81 June 23

Table 7

	LW Radiative Processes	Constant LW	LW & SW Radiative Processes	Imposed Lifting
Chen & Cotton	0%	No	No	No
Chin	11%	No	-7%	No
Tripoli & Cotton	N. A.	No	N.A.	No
Tao *et al.* 1995	8%	8%	-6%	No
Chin *et al.*	15%	No	-18%	2 cm/s Continuous
Fu *et al.*	5%	15%	-1%	8-14 cm/s Not Continous
Xu & Randall	N. A.	N. A.	N. A.	8-14 cm/s Continuous
Tao *et al. 1991*	20%	No	No	4 cm/s Not Continous
Tao *et al. 1995*	36%	2%	-7%	7 cm/s Not Continous
Dharssi *et al*	30%	No	No	7 cm/s Not Continous
Dudhia	36%	No	No	No
Churchill & Houze	0%	No	0%	Strong/ Continuous
Miller & Frank	No	34%**	18-21%**	Strong/ Continuous

Table 8

Altitude Range (m)	Zipser and LeMone		Two-D			Three-D		
	Draft	Core	Cloudy	Active $1ms^{-1}$	Active $2ms^{-1}$	Cloudy	Active $1ms^{-1}$	Active $2ms^{-1}$
9500			1.36 (34.6/25.4)	2.92 (2.98/1.02)	8.00 (1.60/0.20)	1.60 (45.9/28.8)	1.98 (2.67/1.35)	8.60 (1.54/0.18)
4300-8100	0.57 (16.9/29.9)	2.56 (4.6/1.8)	1.04 (11.3/10.9)	2.80 (4.2/1.5)	12.70 (2.8/0.22)	0.81 (11.7/14.4)	2.87 (4.3/1.5)	22.20 (2.89/0.13)
2500-4300	0.60 (18.3/30.3)	1.30 (2.1/1.1)	0.75 (8.4/11.2)	1.05 (4.1/3.9)	2.45 (2.7/1.1)	0.58 (8.3/14.3)	1.23 (3.8/3.1)	7.21 (2.81/0.39)
700-2500	0.65 (16.3/25.2)	1.91 (2.1/1.1)	1.07 (13.9/12.9)	1.37 (4.1/3.0)	2.63 (2.1/0.8)	0.76 (13.4/17.0)	1.72 (4.3/2.5)	4.90 (2.45/0.50)
300-700	0.88 (16.6/18.8)	1.88 (1.5/0.8)	1.13 (15.3/13.5)	1.24 (2.47/2.00)	2.03 (0.73/0.36)	0.95 (17.2/18.2)	1.68 (3.2/1.9)	3.40 (0.85/0.25)
0-300	1.01 (15.9/15.7)	1.50 (0.3/0.2)	1.11 (15.6/14.0)	1.36 (0.87/0.64)	1.78 (0.16/0.09)	0.99 (17.6/17.8)	1.38 (1.1/0.8)	1.20 (0.12/0.10)

R
(U/D)

U = Updraft area coverage in %
D = Downdraft area coverage in %
R = U/D (Ratio between updraft area coverage and downdraft area coverage)

Table 9

TOGA COARE (December 19-26, 1992) (a)

	December 19-26	December 19-20, 23-24 and 25-26	December 20-23 and 24-25
Total Sfc Rainfall (mm)	153.9	29.06	124.84
Stratiform Amount (%)	45%	42%	55%
Evaporation/Condensation	71%	80%	69%
Sublimation/Deposition	50%	56%	48%
Deposition/Condensation	39%	39%	39%

GATE (September 2-8, 1974) (b)

	September 2-8	**Slow Moving September 2-4**	**Fast-Moving 4-6**	**Random 6-8**
Total Sfc Rainfall (mm)	91.46	43.34	39.62	8.50
Stratiform Amount (%)	32%	27%	26%	44%
Evaporation/Condensation	54%	58%	44%	68%
Sublimation/Deposition	32%	36%	27%	24%
Deposition/Condensation	22%	23%	25%	9.5%

Table 10

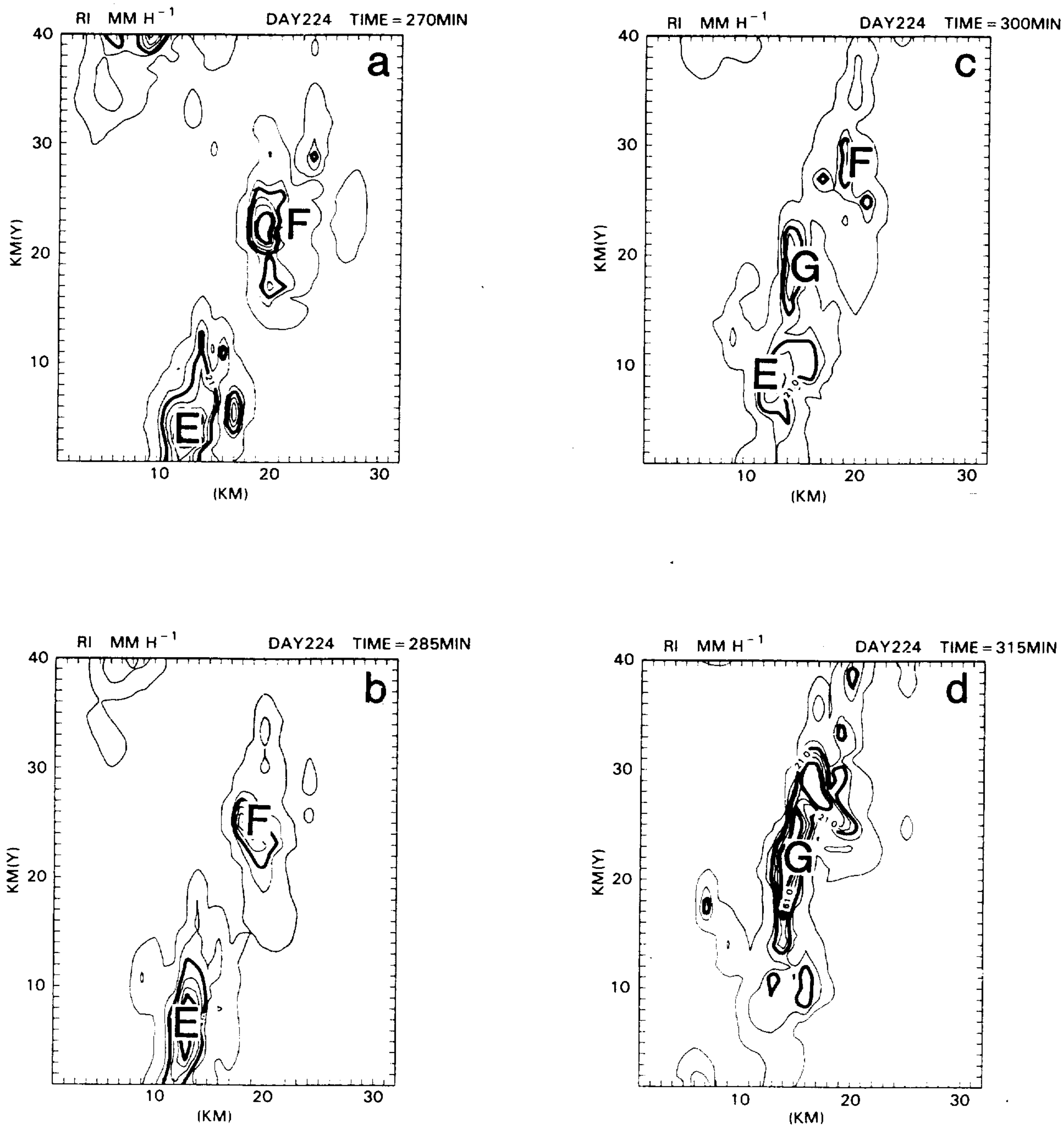
RI MM H^{-1} DAY224 TIME = 270MIN
a
RI MM H^{-1} DAY224 TIME = 300MIN
c
RI MM H^{-1} DAY224 TIME = 285MIN
b
RI MM H^{-1} DAY224 TIME = 315MIN
d
E
F
G
KM(Y)
(KM)
10
20
30
40

Fig. 1

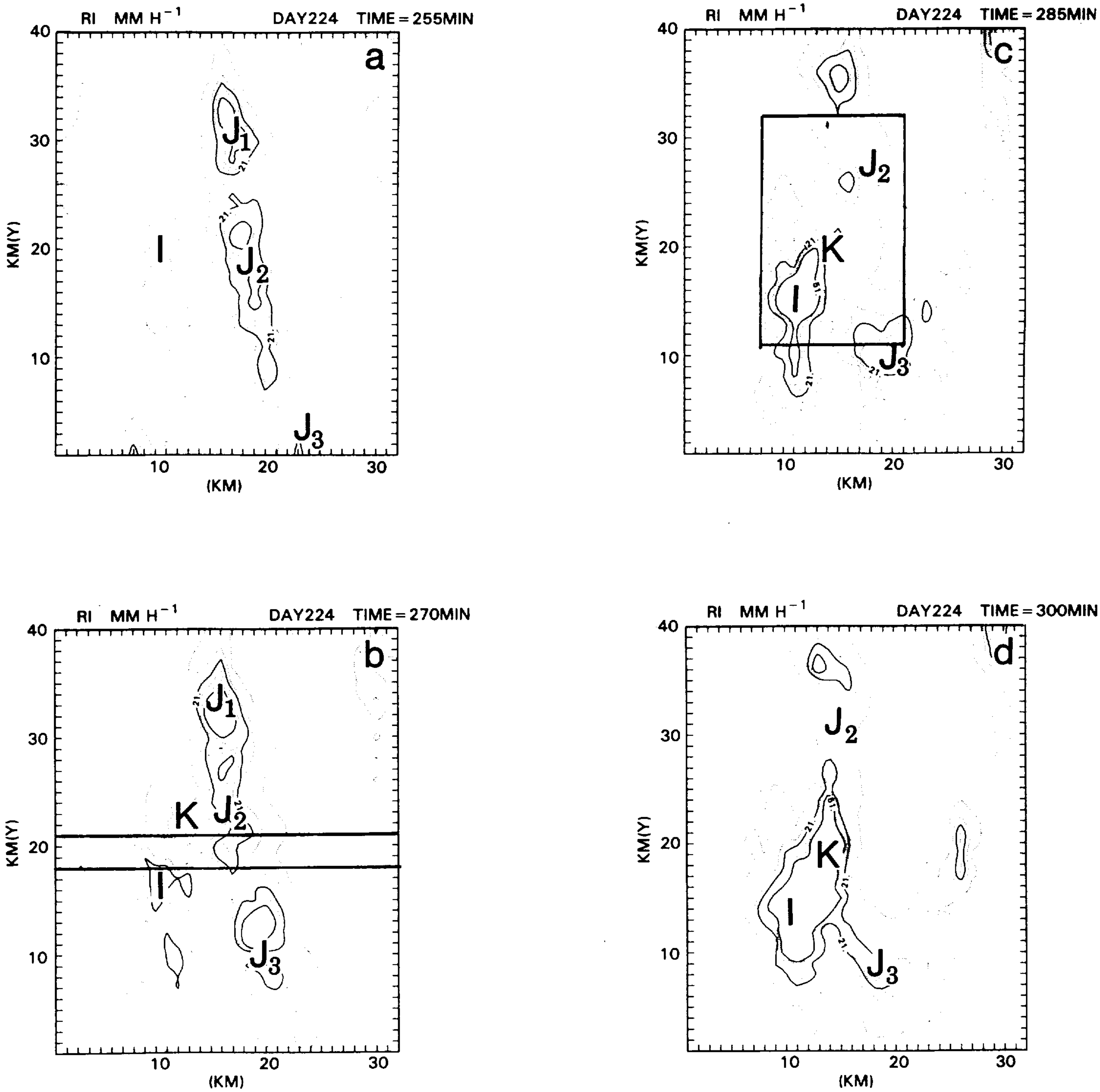
RI MM H^{-1} DAY224 TIME=255MIN
a
J1
J2
J3
I
KM(Y)
(KM)
RI MM H^{-1} DAY224 TIME=285MIN
c
J2
K
I
J3
RI MM H^{-1} DAY224 TIME=270MIN
b
J1
K
J2
I
J3
RI MM H^{-1} DAY224 TIME=300MIN
d
J2
K
I
J3

Fig. 2

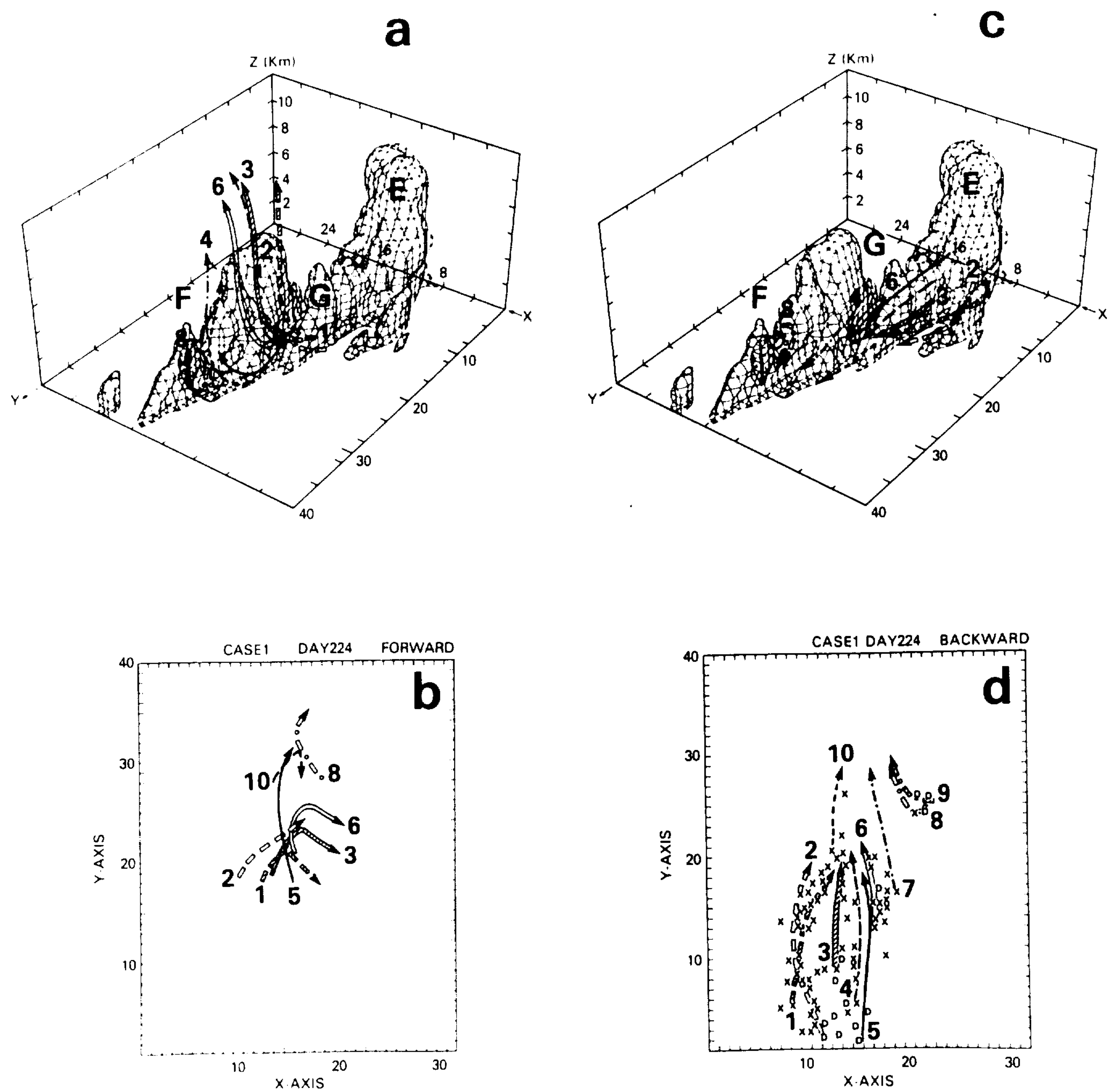
a
Z (Km)
10
8
6
4
2
24
16
8
X
Y
10
20
30
40
E
F
G
1
2
3
4
6
c
Z (Km)
10
8
6
4
2
24
16
8
X
Y
10
20
30
40
E
F
G
2
6
8
b
CASE1 DAY224 FORWARD
Y-AXIS
X-AXIS
40
30
20
10
10
20
30
1
2
3
5
6
8
10
d
CASE1 DAY224 BACKWARD
Y-AXIS
X-AXIS
40
30
20
10
10
20
30
1
2
3
4
5
6
7
8
9
10

Fig. 3

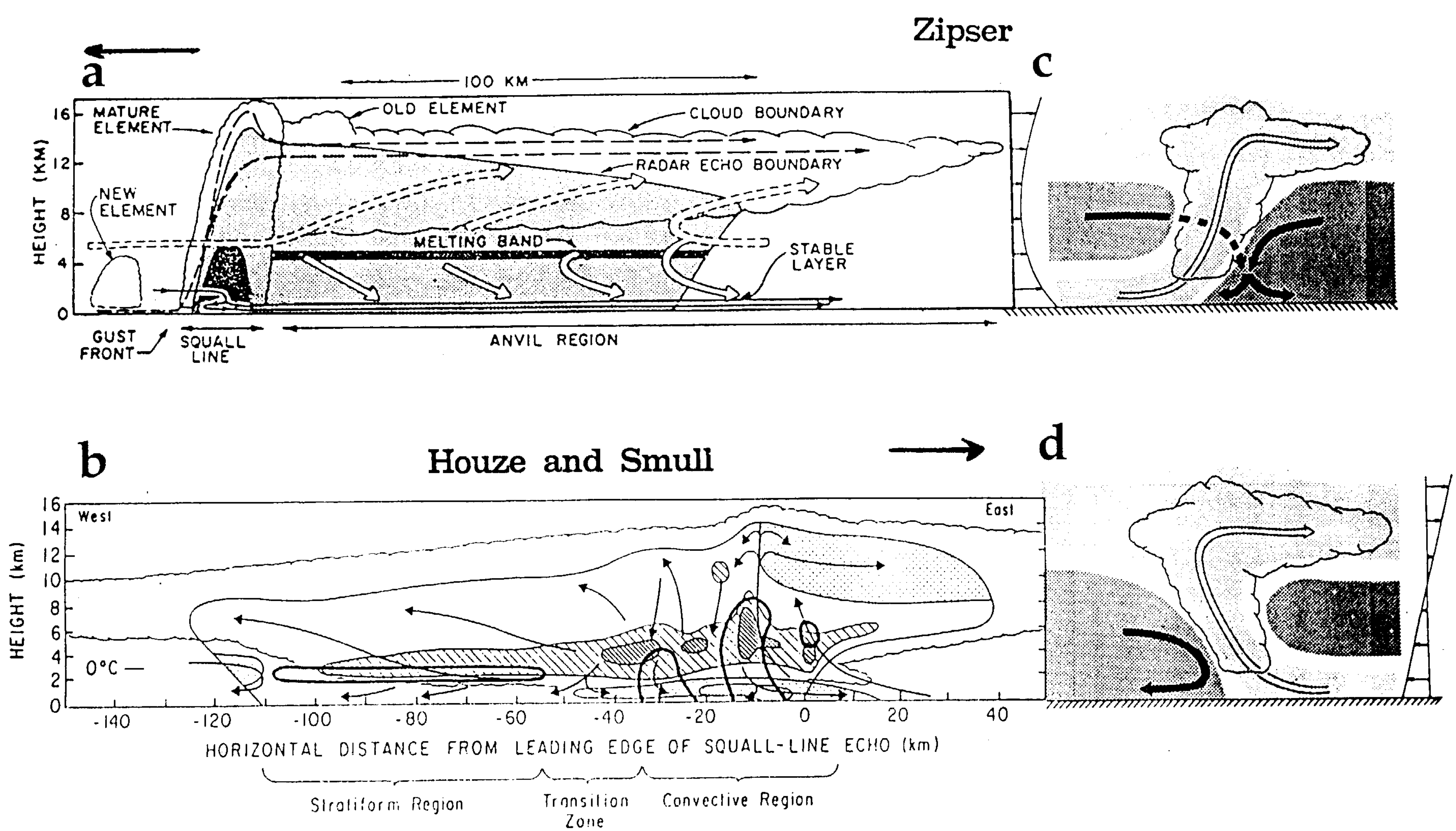
Zipser
a
b
c
d
Houze and Smull
100 KM
MATURE ELEMENT
OLD ELEMENT
CLOUD BOUNDARY
RADAR ECHO BOUNDARY
NEW ELEMENT
MELTING BAND
STABLE LAYER
GUST FRONT
SQUALL LINE
ANVIL REGION
HEIGHT (KM)
16
12
8
4
0
West
East
0°C
HEIGHT (km)
HORIZONTAL DISTANCE FROM LEADING EDGE OF SQUALL-LINE ECHO (km)
Stratiform Region
Transition Zone
Convective Region
-140
-120
-100
-80
-60
-40
-20
0
20
40

Fig. 4

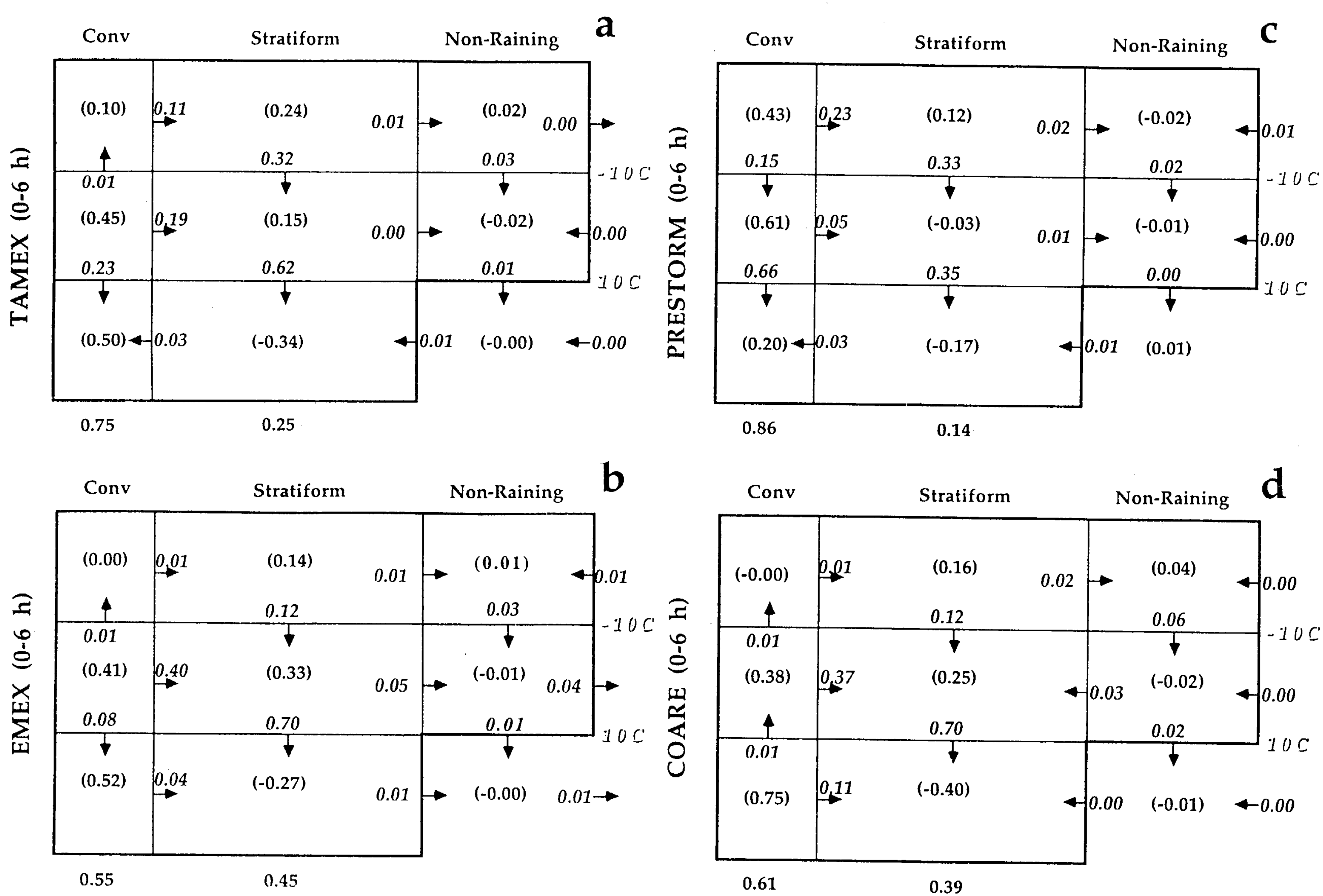
a
b
c
d
Conv
Stratiform
Non-Raining
TAMEX (0-6 h)
EMEX (0-6 h)
PRESTORM (0-6 h)
COARE (0-6 h)
-10 C
10 C
(0.10)
0.11
(0.24)
0.01
(0.02)
0.00
0.01
0.32
0.03
(0.45)
0.19
(0.15)
0.00
(-0.02)
0.00
0.23
0.62
0.01
(0.50)
0.03
(-0.34)
0.01
(-0.00)
0.00
0.75
0.25
(0.00)
0.01
(0.14)
0.01
(0.01)
0.01
0.01
0.12
0.03
(0.41)
0.40
(0.33)
0.05
(-0.01)
0.04
0.08
0.70
0.01
(0.52)
0.04
(-0.27)
0.01
(-0.00)
0.01
0.55
0.45
(0.43)
0.23
(0.12)
0.02
(-0.02)
0.01
0.15
0.33
0.02
(0.61)
0.05
(-0.03)
0.01
(-0.01)
0.00
0.66
0.35
0.00
(0.20)
0.03
(-0.17)
0.01
(0.01)
0.86
0.14
(-0.00)
0.01
(0.16)
0.02
(0.04)
0.00
0.01
0.12
0.06
(0.38)
0.37
(0.25)
0.03
(-0.02)
0.00
0.01
0.70
0.02
(0.75)
0.11
(-0.40)
0.00
(-0.01)
0.00
0.61
0.39

Fig. 5

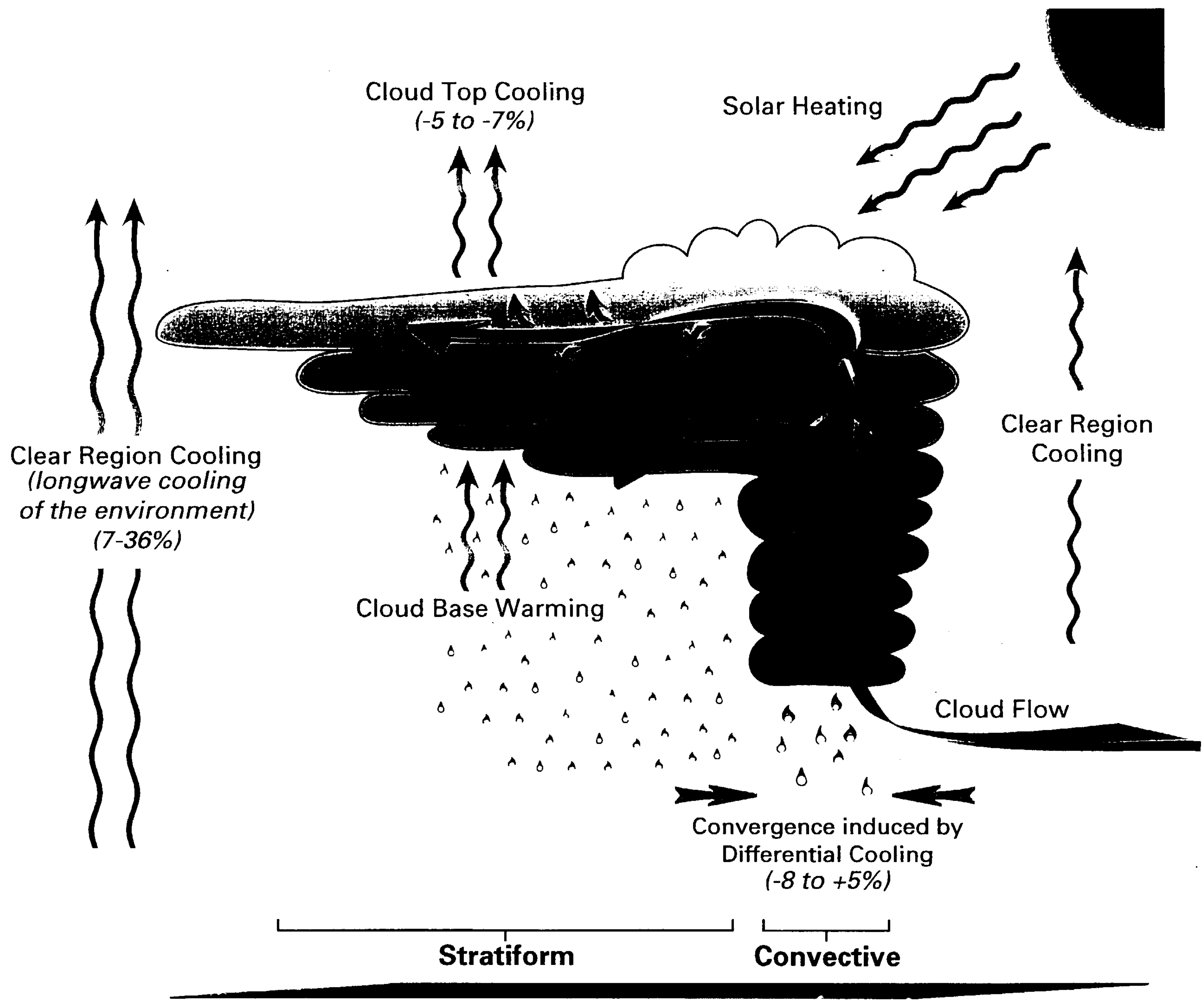
Cloud Top Cooling
(-5 to -7%)
Solar Heating
Clear Region Cooling
(longwave cooling
of the environment)
(7-36%)
Clear Region
Cooling
Cloud Base Warming
Cloud Flow
Convergence induced by
Differential Cooling
(-8 to +5%)
Stratiform
Convective

Fig. 6

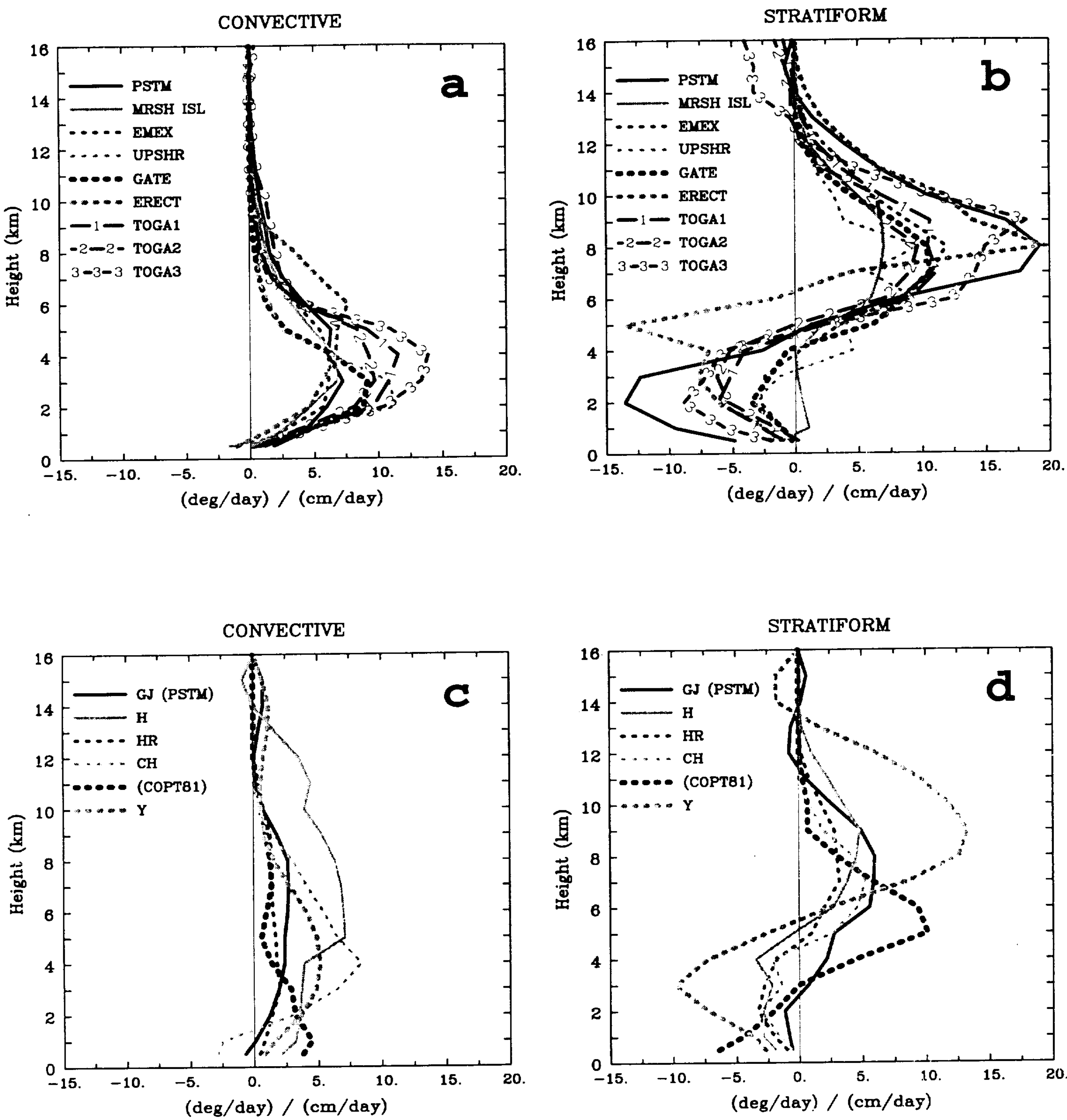
CONVECTIVE
a
PSTM
MRSH ISL
EMEX
UPSHR
GATE
ERECT
TOGA1
TOGA2
TOGA3
Height (km)
(deg/day) / (cm/day)
STRATIFORM
b
PSTM
MRSH ISL
EMEX
UPSHR
GATE
ERECT
TOGA1
TOGA2
TOGA3
Height (km)
(deg/day) / (cm/day)
CONVECTIVE
c
GJ (PSTM)
H
HR
CH
(COPT81)
Y
Height (km)
(deg/day) / (cm/day)
STRATIFORM
d
GJ (PSTM)
H
HR
CH
(COPT81)
Y
Height (km)
(deg/day) / (cm/day)

Fig. 7

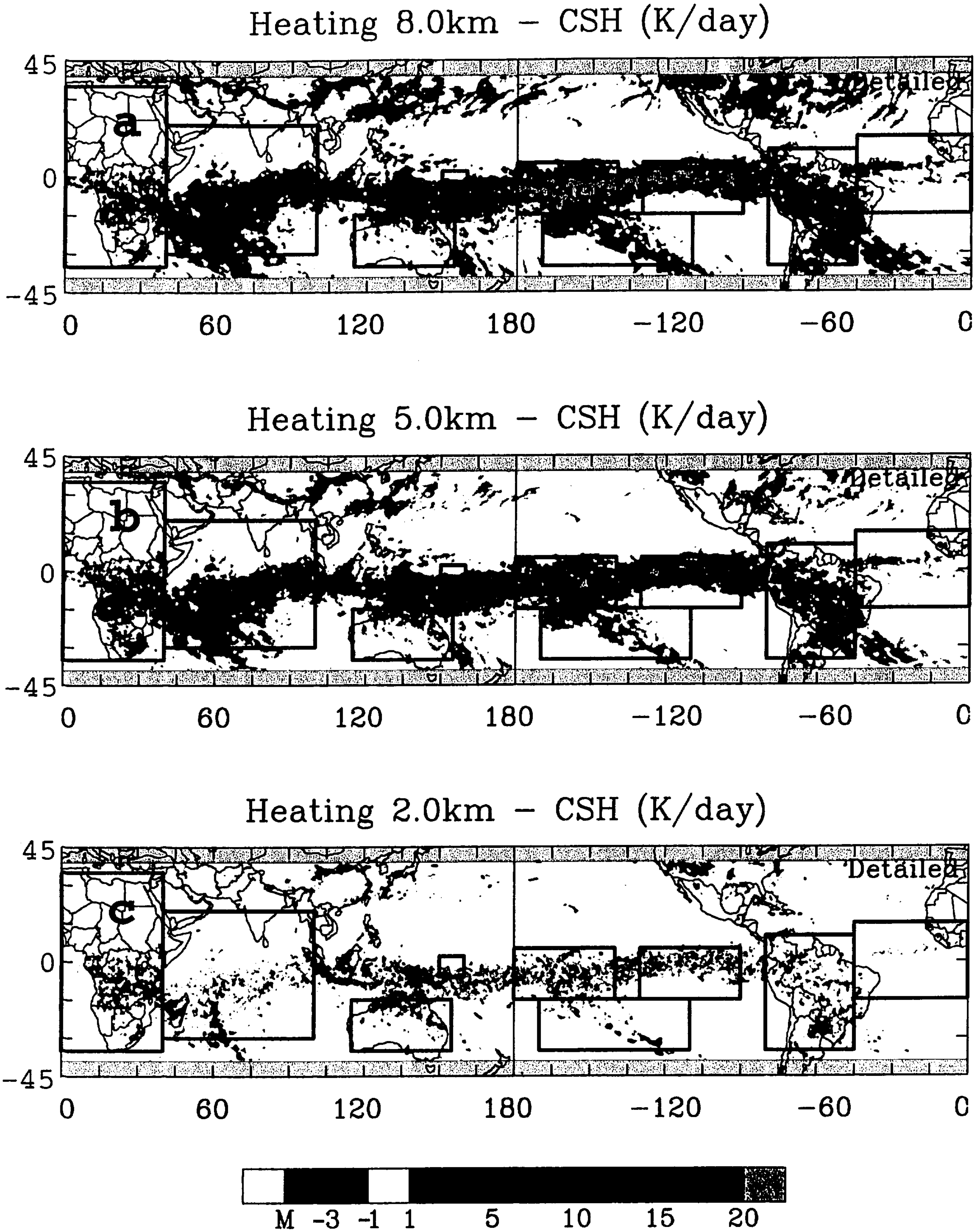

Heating 8.0km - CSH (K/day)
a
Detailed
Heating 5.0km - CSH (K/day)
b
Detailed
Heating 2.0km - CSH (K/day)
c
Detailed
45
0
-45
0
60
120
180
-120
-60
0
M -3 -1 1 5 10 15 20

Fig. 8

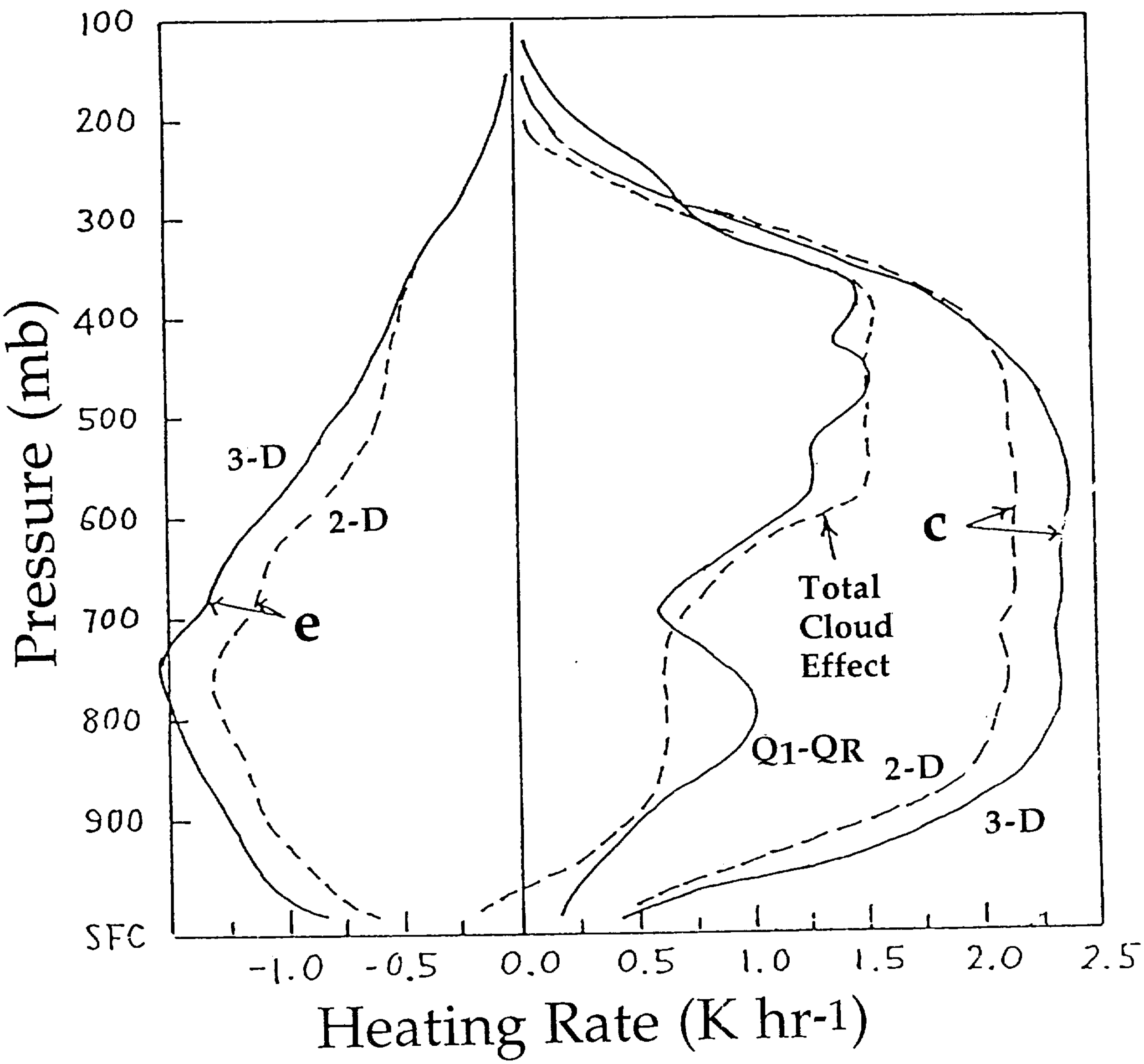

Pressure (mb)
100
200
300
400
500
600
700
800
900
SFC
3-D
2-D
e
Total
Cloud
Effect
c
Q1-QR
2-D
3-D
-1.0
-0.5
0.0
0.5
1.0
1.5
2.0
2.5
Heating Rate (K hr-1)

Fig. 9

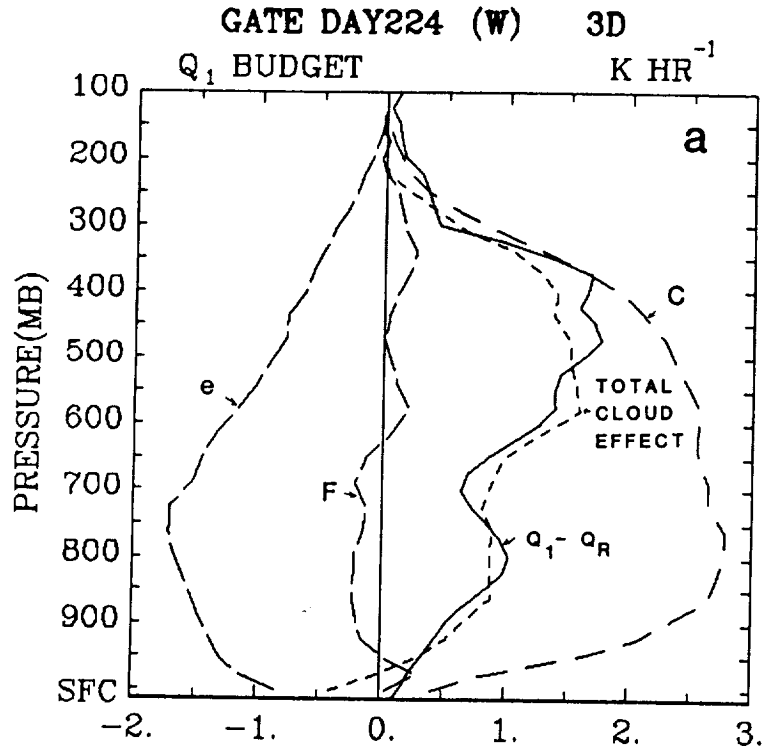
GATE DAY224 (W) 3D
Q1 BUDGET
K HR-1
a
PRESSURE(MB)
100
200
300
400
500
600
700
800
900
SFC
-2.
-1.
0.
1.
2.
3.
e
F
C
TOTAL CLOUD EFFECT
Q1- QR

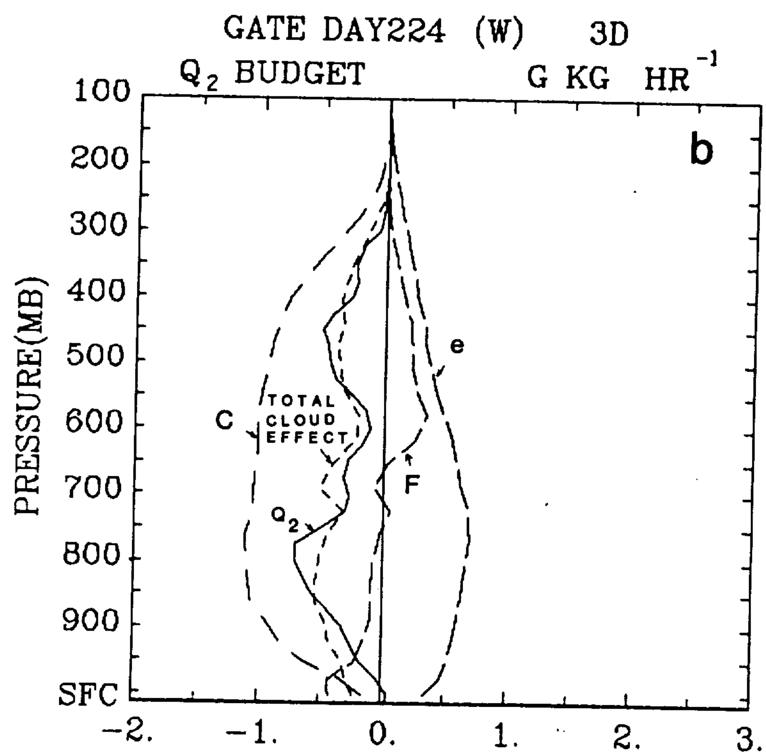
GATE DAY224 (W) 3D
Q2 BUDGET
G KG HR-1
b
PRESSURE(MB)
100
200
300
400
500
600
700
800
900
SFC
-2.
-1.
0.
1.
2.
3.
e
C
TOTAL CLOUD EFFECT
F
Q2

Fig. 10

(a) (b)

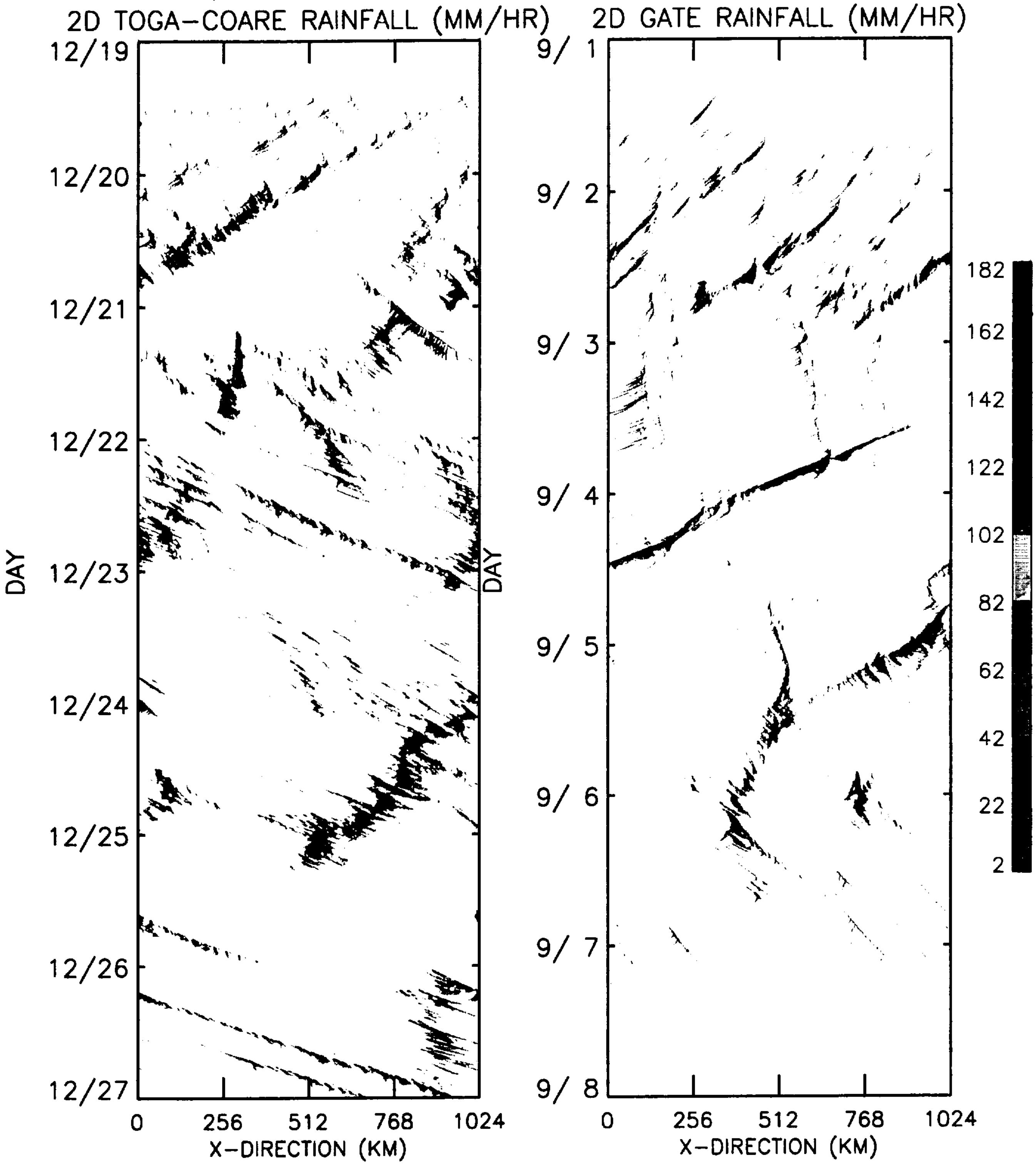
2D TOGA-COARE RAINFALL (MM/HR)
2D GATE RAINFALL (MM/HR)
DAY
12/19
12/20
12/21
12/22
12/23
12/24
12/25
12/26
12/27
9/ 1
9/ 2
9/ 3
9/ 4
9/ 5
9/ 6
9/ 7
9/ 8
0
256
512
768
1024
X-DIRECTION (KM)
182
162
142
122
102
82
62
42
22
2

Fig. 11